Climate Data Record (CDR) Program

Climate Algorithm Theoretical Basis Document (C-ATBD)

Sea Ice Concentration

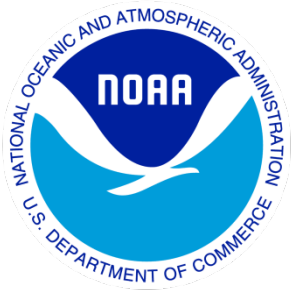

CDR Program Document Number: CDRP-ATBD-0107
Configuration Item Number: 01B-11 and 01B-11a
Revision 12 / January 15, 2026

REVISION HISTORY

Rev.	Author	DSR No.	Description	Date
1	Walt Meier, Research Scientist, NSIDC	DSR-112	Initial release.	09/20/2011
2	Walt Meier, Research Scientist, NSIDC	DSR-204	Added description of monthly files and memory allocations for processing. Sections 3.2, 3.4.4, and 5.6.	05/29/2012
3	Walt Meier, Research Scientist, NSIDC	DSR-411	Changes made to describe Version 2 Revision 0 of the CDR. Sections 3.2, 3.3.1, 3.4.1.4, 3.4.4.1, 3.4.4.2, and 5.6. 6.1.4 (deleted)	03/26/2013
4	Ann Windnagel, Professional Research Assistant, NSIDC	DSR-920	Changes made to describe Version 2 Revision 1 of the CDR. Updated Figures 2 and 5 in Section 3.2, Sections 1.3 and 5.6, and Table 12.	09/19/2015
5	Ann Windnagel, Professional Research Assistant, NSIDC	DSR-1148	Changes made to describe Version 3 and the near-real-time portion of the time series: Updated sections 1.1, 2.1, 2.2, 3, 4, 5.6, 6, and 8.	09/14/2017
6	Ann Windnagel, Professional Research Assistant, NSIDC	DSR-1216	Changes made to describe Version 3 Revision 1. Updated sections 3.2, 3.3, and 3.4. Changes made to address Version 3.1: Updated section 3.3.1.	12/20/2017
7	Ann Windnagel, Professional Research Assistant, NSIDC	DSR-1240	Changes made to tables 3, 4, and 5: instruments for the input data were changed from SMMIS and SMM/I to SSMIS and SSM/I.	03/06/2018
8	Ann Windnagel, Professional Research Assistant, NSIDC	DSR-1525	Made major updates to the entire document to reflect the new Version 4 TCDR and Version 2 ICDR release.	04/19/2021
9	Ann Windnagel, Professional Research Assistant, NSIDC	DSR-1527	Minor revision due to typographical errors.	06/03/2021

10	Ann Windnagel, Professional Research Assistant, NSIDC	DSR-1546	Made significant updates to Quality Control Procedures section to the temporal interpolation and NT weather filters text so that it matches what the code is producing. Made significant updates to the Future Enhancements section with new enhancements and deleted the enhancements we just completed.	06/23/21
11	Ann Windnagel, Professional Research Assistant, NSIDC	DSR-2005	Major revision of entire document to reflect changes with the new Version 5 TCDR and Version 3 ICDR.	12/12/2024
12	Ann Windnagel, Senior Professional Research Assistant, NSIDC	DSR-2645	Major revision of entire document to reflect changes with the new Version 6 TCDR and Version 4 ICDR	01/15/2026

TABLE of CONTENTS

LIST of FIGURES

LIST of TABLES

Introduction

1.1 Purpose

The purpose of this document is to describe the sea ice concentration (SIC) algorithm that is used to produce a climate data record of sea ice concentration for the NOAA Climate Data Record (CDR) program. An overview of research that led to the algorithm can be found in Meier et al. 2014 and in other papers led by Meier, while Peng et al. (2013) summarize how the algorithm data record supports climate applications.

The NOAA program at the National Snow and Ice Data Center (NSIDC) maintains the SIC CDR. Beginning in 2015, updates to this document are submitted to NOAA National Centers for Environmental Information (NCEI) by Ann Windnagel, CDR Product Owner at NSIDC.

The SIC CDR algorithm is used to create sea ice concentrations from passive microwave data from the Scanning Multichannel Microwave Radiometer (SMMR) on the Nimbus 7 satellite, the Special Sensor Microwave/Imager (SSM/I) and the Special Sensor Microwave Imager and Sounder (SSMIS) sensors on U.S. Department of Defense Meteorological Satellite Program (DMSP) platforms, and the Advanced Microwave Scanning Radiometer 2 (AMSR2) sensor onboard the Japan Aerospace Exploration Agency (JAXA) Global Change Observation Mission - W1 (GCOM-W1) satellite.

The goal of the SIC CDR is to provide a consistent, reliable, and well-documented product that meets CDR guidelines as defined in *Climate Data Records from Environmental Satellites* (NAS, 2004). NSIDC supplies this data product in two parts: (1) a Thematic Climate Data Record (TCDR) product (G02202 V6) titled the *NOAA/NSIDC Climate Data Record of Passive Microwave Sea Ice Concentration, Version 6* (Meier et al., 2026a), that undergoes complete spatial and temporal gap filling; and (2) an Interim Climate Data Record (ICDR) product (G10016 V4) titled the *Near-Real-Time NOAA/NSIDC Climate Data Record of Passive Microwave Sea Ice Concentration, Version 4* (Meier et al., 2026b), that goes through initial spatial and temporal gap filling. We make the NRT product available to users until the release of the finalized Sea Ice Concentration CDR (NOAA data set ID 01B-11, NSIDC data set ID G02202), which, with the release of this new version, is available with an approximate 1-week latency.

With the release of SIC CDR Version 6, the record now uses brightness temperature data from the AMSR2 instrument as input beginning 1 January 2025. There are two reasons for this change. First, the DMSP satellites are aging and are slated to be decommissioned no later than October 2026. It is important to ensure the continuation of a quality-controlled sea ice concentration time series. Therefore, we switched to the AMSR2 sensor to continue the sea ice concentration record. Furthermore, the AMSR2 instrument is a next-generation sensor with better spatial resolution than its predecessor SSM/I and SSMIS instruments. The differences between the SSMIS and AMSR2

sensors required intercalibrating the AMSR2 record with the historical record for consistency. See section 3.4.3 for more information.

The algorithm is defined by the computer program (code) that accompanies this document; and thus, the intent here is to provide a guide to understanding that algorithm, from both a scientific perspective and a software engineering perspective.

1.2 Definitions

The following symbols are used throughout this document:

T_B = *brightness temperature* = $\varepsilon * T$ (1)
ε = *emissivity* (2)
T = *physical temperature* (3)
T_O = *brightness temperature for open water* (4)
T_I = *brightness temperature for 100% sea ice* (5)
PR = *polarization ratio* (6)
GR = *gradient ratio* (7)

1.3 Referencing and Citing this Document

This document may be referred to as follows:

Sea Ice Concentration - Climate Algorithm Theoretical Basis Document (C-ATBD), NOAA Climate Data Record Program CDRP-ATBD-0107 Rev. 12 (2025). Available at https://www.ncei.noaa.gov/products/climate-data-records.

However, when citing this document in a research paper, please use the following:

Windnagel, A., Meier, W. N., Fetterer, F., & Stewart, S. (2026). Sea Ice Concentration - Climate Algorithm Theoretical Basis Document (C-ATBD), NOAA Climate Data Record Program CDRP-ATBD-0107, Rev. 12. NOAA NCEI CDR Program.

1.4 Document Maintenance

This is the ATBD for the NOAA/NSIDC Climate Data Record of Passive Microwave Sea Ice Concentration, Version 6, Revision 0.

2. Observing Systems Overview

2.1 Products Generated

The primary product is the SIC CDR. The algorithm that produces the data record uses gridded brightness temperatures (TBs) from several passive microwave instruments: the Nimbus-7 SMMR, the DMSP series of SSM/I and SSMIS instruments, and the JAXA AMSR2 instrument on GCOM-W1. The SIC CDR data are estimates of sea ice concentration beginning in October 1978 produced by combining concentration estimates from two algorithms developed at the NASA Goddard Space Flight Center (GSFC): the NASA Team (NT) algorithm (Cavalieri et al., 1984) and the Bootstrap (BT) algorithm (Comiso, 1986). These algorithms are described in Section 3, and Section 3.3 provides information on the input brightness temperatures.

Accompanying the concentration estimates are data quality information fields. One field is a concentration standard deviation of the mean that indicates local spatial variance. Grid cells with higher standard deviation values have lower confidence levels. Another field includes quality information such as melt state and proximity to the coast. We have less confidence in values from grid cells after melt has started or that are relatively close to the coast.

2.2 Instrument Characteristics

Six instruments are used in the generation of the SIC CDR time series. Table 1 lists the instruments and their orbital characteristics, while Table 2 lists the pertinent channels, their frequencies, field of view, swath width, and Earth incidence angle.

The NASA SMMR passive microwave sensor was launched aboard the Nimbus-7 satellite in October 1978. The ten-channel SMMR sensor measured orthogonally polarized – horizontal (H) and vertical (V) – antenna temperature data in five microwave frequencies (Gloersen and Hardis, 1978). Only four of these channels are used for the SIC CDR: 18.0 GHz (V/H) and 37.0 GHz (V/H). The SMMR brightness temperature record provides every-other-day concentration estimates.

The first SSM/I sensor was launched aboard the DMSP-F8 mission in 1987 (Hollinger et al., 1990). A series of SSM/I conically-scanning sensors on subsequent DMSP satellites has provided a continuous data stream since then. However, only SSM/I sensors on the DMSP-F8, -F11, and -F13 platforms are used in the generation of the CDR. The SSM/I sensor has seven channels at four frequencies. The ones used in SIC CDR processing are 19.4 GHz (V/H), 22.2 GHz (V), and 37.0 GHz (V/H).

Beginning with the launch of F16 in 2003, the SSM/I sensor was replaced by the SSMIS sensor. The SSMIS sensor has 24 channels (Kunkee et al., 2008) but the same 19.4 GHz (V/H), 22.2 GHz (V), and 37.0 GHz (V/H) channels are used in the generation of the SIC CDR. Only the F17 SSMIS instrument is used for SIC CDR processing.

AMSR2 was launched aboard GCOM-W1 on 18 May 2012 with 16 channels. It has channel frequencies like those of the SMMR, SSM/I, and SSMIS instruments. The AMSR2 channels used to process the AMSR2 sea ice concentrations are the 18.7 GHz (V/H), 23.8 GHz (V), and 36.5 GHz (V/H) channels.

For simplicity in this document, the channels are denoted as simply 19 (V/H) for the 18.0/18.7/19.4 GHz channels, 22V for the 21.0/22.2/23.8 GHz channels, and 37 (V/H) for the 36.5/37.0 GHz channels. Depending on the platform, the satellite altitudes are 700 km to 955 km and sensor (earth incidence) angles are 50.2° to 55.0° (Table 1).

Satellite	Launch Date (YYYY-MM-DD)	Nominal Altitude (km)	Inclination Angle (degrees)	Orbital Period (minutes)	Ascending Node Equatorial Crossing Time at Launch (approximate local time to the nearest half hour)
Nimbus-7	1978-10-24	955	99.1	104	12:00
DMSP-F8	1987-06-18	860	98.8	102	06:00
DMSP-F11	1991-11-28	830	98.8	101	17:30
DMSP-F13	1995-03-24	850	98.8	102	17:30
DMSP-F17	2006-11-04	855	98.8	102	17:30
GCOM-W1	2012-05-18	700	98.2	98.8	13:30

Table 1: Comparison of Nimbus, DMSP, and GCOM-W1 orbital parameters

Polar orbits and wide swaths provide near-complete coverage at least once per day in the polar regions except for a small region around the North Pole called the pole hole. The footprint or instantaneous field of view (IFOV) of the sensors varies with frequency (Table 2). Regardless of footprint size, the channels are gridded onto a 25 km polar stereographic grid.

Satellite	Sensor	Frequencies (GHz)	IFOV (km)	Swath Width (km)	Earth Incidence Angle (degrees)
NIMBUS-7	SMMR	18.0	55 x 41	783	50.2
		21.0	46 x 30		
		37.0	27 x 18		
DMSP-F8	SSM/I	19.4	69 x 43	1400	53.1
		22.2	60 x 40		

		37.0	37 x 28		
DMSP-F11	SSM/I	19.4	69 x 43	1400	52.8
		22.2	60 x 40		
		37.0	37 x 28		
DMSP-F13	SSM/I	19.4	69 x 43	1400	53.4
		22.2	60 x 40		
		37.0	37 x 28		
DMSP-F17	SSMIS	19.4	72 x 44	1700	53.1
		22.2	72 x 44		
		37.0	44 x 26		
GCOM-W1	AMSR2	18.7	14 x 22 (L1R 62 x 35)	1450	55.0
		23.8	15 x 26 (L1R 62 x 35)		
		36.5	7 x 12 (L1R 42 x 25)		

Table 2: Instrument characteristics of SMMR, SSM/I, SSMIS, and AMSR2 and frequencies used in the SIC CDR algorithm (Gloersen and Barath, 1977; Hollinger et al., 1990; Kunkee et al., 2008; T. Kawanishi *et al*., 2003; Nakagawa, 2010). Note for AMSR2: Both the original and L1R resolutions are shown. L1R data are used in the CDR. See Section 3.3 for more information.

3. Algorithm Description

3.1 Algorithm Overview

The Sea Ice Concentration CDR algorithm uses estimates of ice coverage derived at NSIDC from the NASA Team (Cavalieri et al., 1984) and Bootstrap (Comiso, 1986) algorithms as input and merges them into a combined single concentration estimate based on the known characteristics of the two algorithms. The sea ice concentrations estimated by the Bootstrap algorithm are analyzed first. Any grid cell with a concentration estimate of 10% or greater will be considered valid ice in the final product. For each grid cell that passes the Bootstrap threshold, the concentration value given by the NASA Team algorithm is compared with that given by the Bootstrap algorithm; whichever value is greater is selected as the CDR value. The reasons behind this approach are discussed in Section 3.4.1.3.

Automated quality control measures are implemented on the SIC CDR after merging the NASA Team and Bootstrap concentrations. This includes applying a set of invalid ice masks to screen out errant retrievals of ice in regions where sea ice has not occurred in the past few decades. In addition, two weather filters – a BT weather filter and an NT weather filter – that are based on ratios of channels sensitive to enhanced emission over open water are applied to filter weather effects. Finally, two land-spillover corrections (The NASA Team 2 and the BT) are used to filter out much of the erroneous

coastal ice that results from mixed land-ocean grid cells. These are described in section 3.4.1.4.

3.2 Processing Outline

The following flow diagram (Figure 1) describes an overview of the Python code used for processing the finalized daily and monthly TCDR sea ice concentrations and the near-real-time provisional daily and monthly ICDR sea ice concentrations. See Section 5.2 for information on how to access the source code.

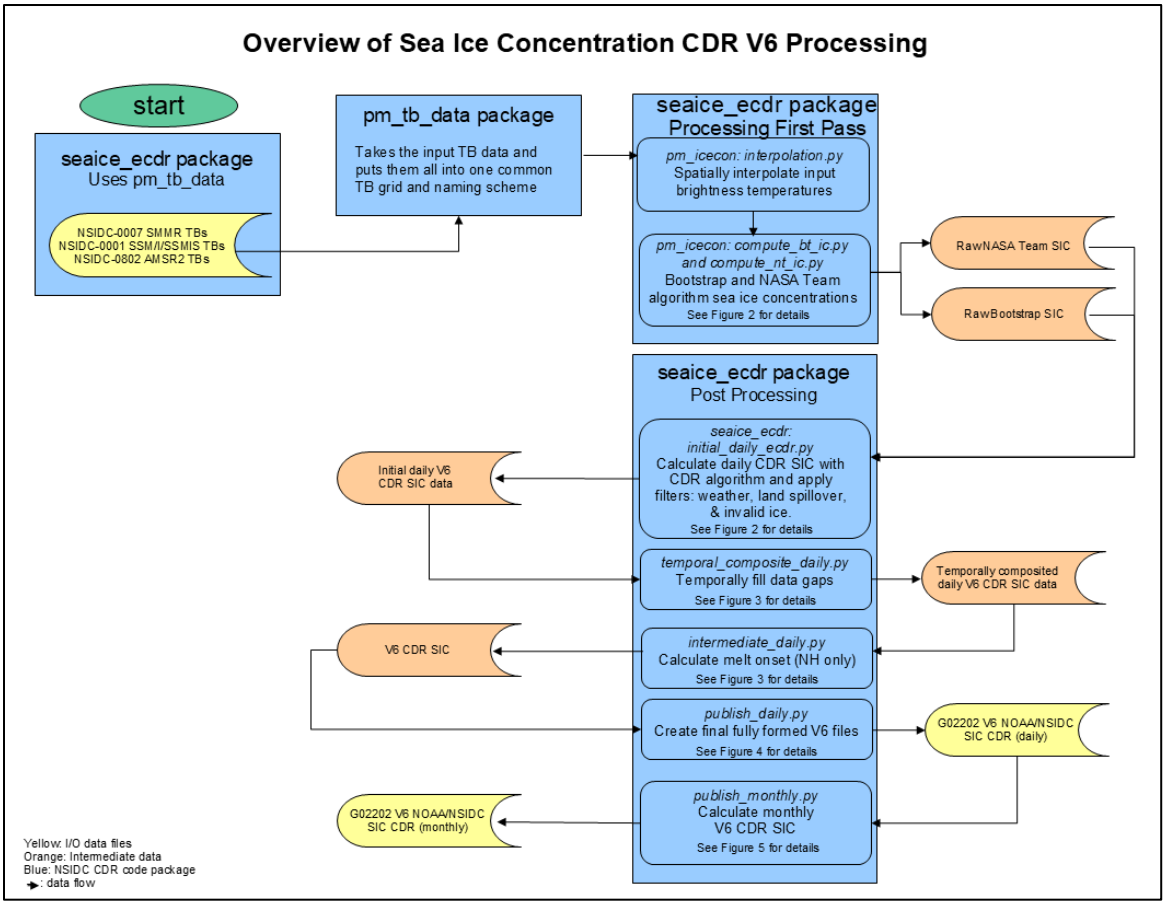

Figure 1: Flowchart showing the overview of SIC TCDR and ICDR processing. Note that the ICDR is identical in processing except that the output is G10016 V4.

3.2.1 Daily Processing

The following flow diagrams (Figure 2, Figure 3, and Figure 4) describe the processing of the daily TCDR and ICDR sea ice concentration products.

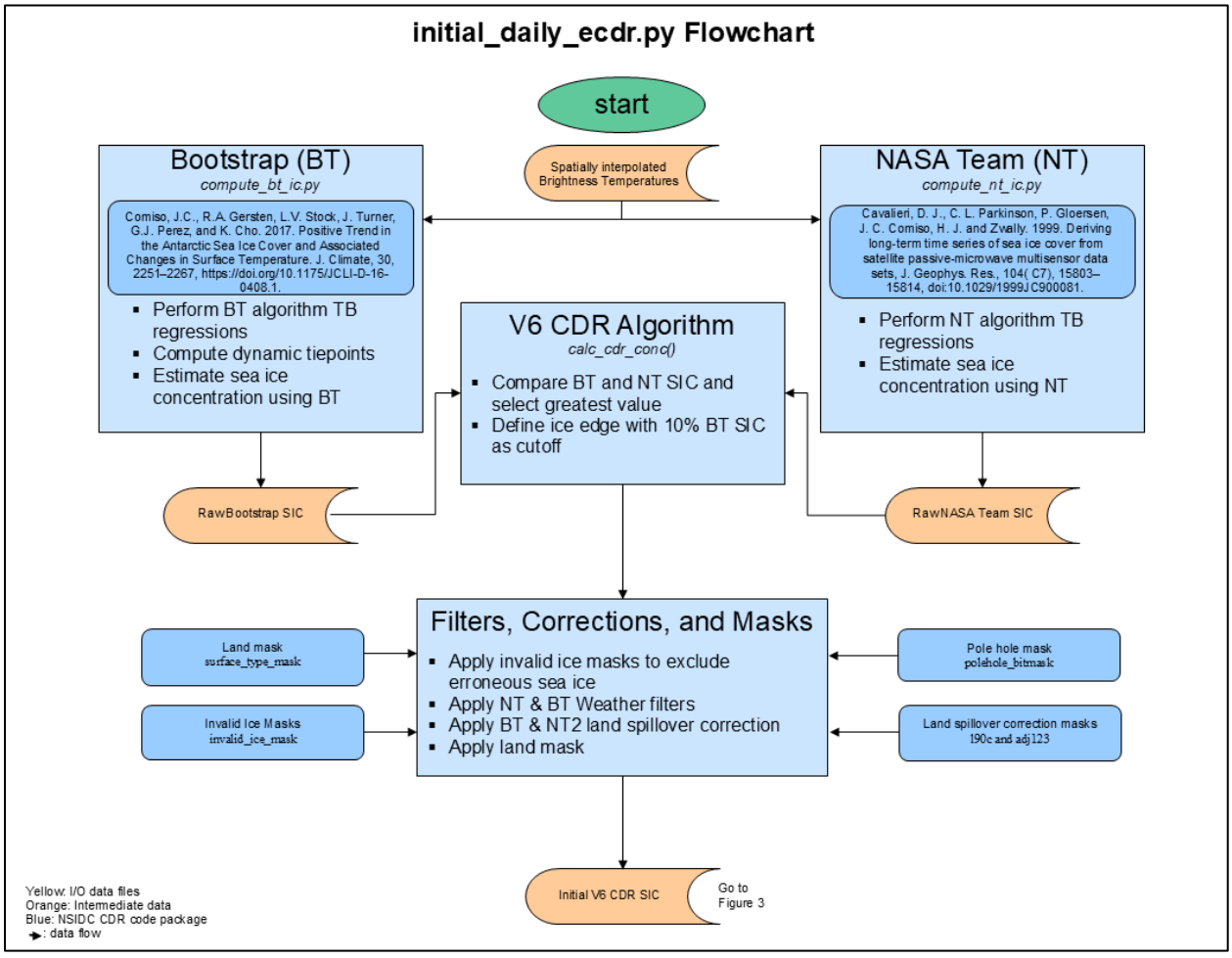

Figure 2: Overview of main python code for the initial daily SIC TCDR and ICDR processing showing the Bootstrap and NASA Team processing. Note that the ICDR is identical in processing except that the output is G10016 V4.

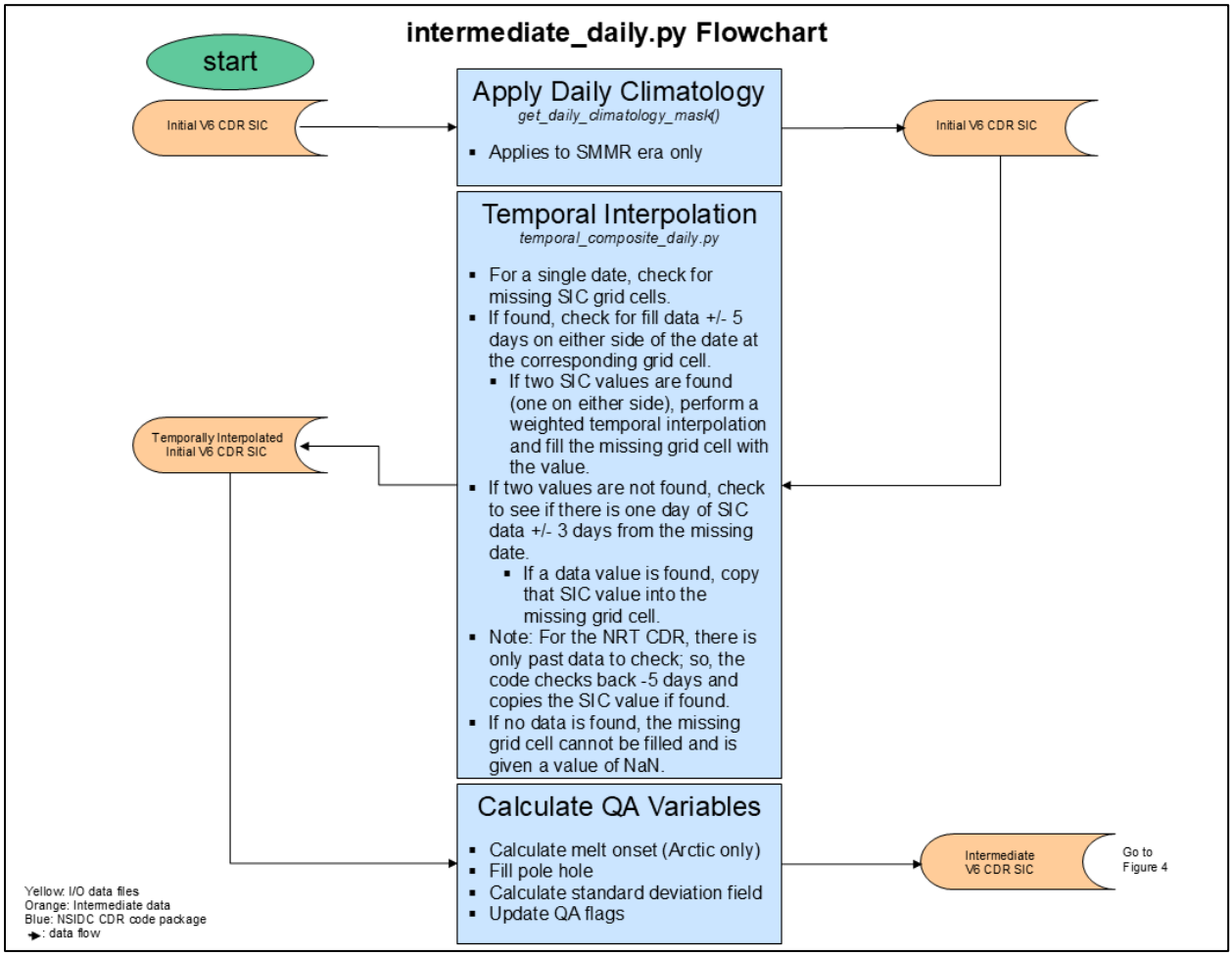

Figure 3: Overview of the code for the intermediate daily TCDR and ICDR processing code. Note that the ICDR is identical except that for the temporal interpolation, the code only looks back 5 days and the output is G10016 V4.

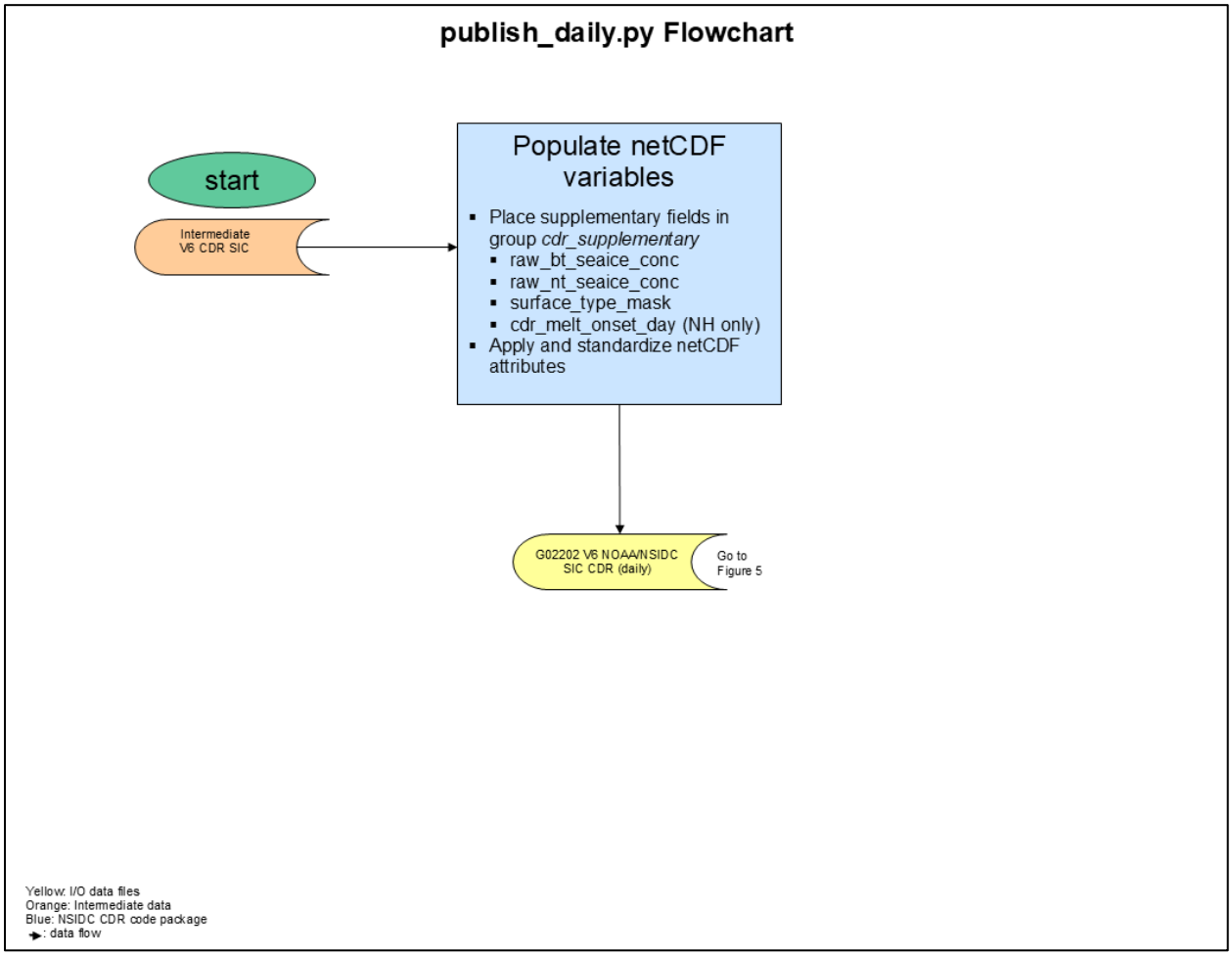

Figure 4. Overview of the code for the published daily TCDR and ICDR processing code. Note that the ICDR is identical in processing except that the output is G10016 V4.

3.2.2 Monthly Processing

The following flow diagram (Figure 5) describes the processing of the monthly CDR sea ice concentration for the finalized TCDR data and the near-real-time ICDR data.

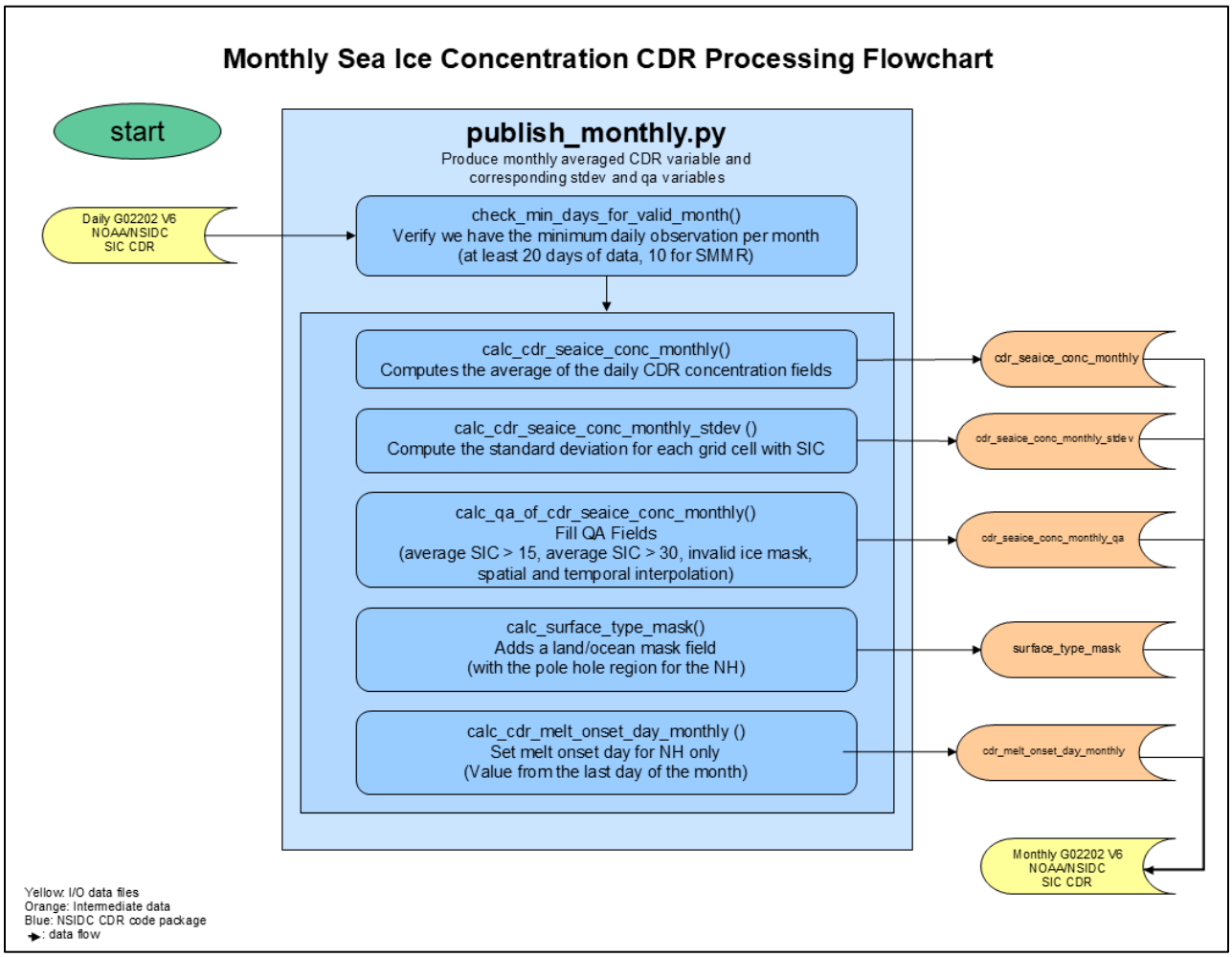

Figure 5: Monthly TCDR and ICDR processing. Note that the ICDR processing is identical except that the input data is the daily G10016 V4 data and the output is G10016 V4 monthly data.

3.3 Algorithm Input

3.3.1 Primary Sensor Data

The primary input data are calibrated and gridded brightness temperatures produced by NSIDC from the Nimbus-7 SMMR, the DMSP SSM/I, the DMSP SSMIS, and the GCOM-W1 AMSR2 passive microwave sensors. Note that for AMSR2, NSIDC uses the Level 1R (L1R) product from JAXA, which has been resampled to a lower resolution by JAXA (See Table 2 for IFOVs). NSIDC chose to use these resampled data because

they better match the lower resolution SSMIS instrument and allow for better continuity in the time series. See Table 3 for a list of the sensors, their dates, and the URL to the input data product. Table 2 lists the channels used. The choice of these satellites keeps the equatorial crossing times as consistent as possible and thereby minimizes potential diurnal effects in brightness temperature data.

Note: Instead of using JAXA L1R AMSR2 data directly, we use the AMSR2 Daily Polar Gridded Brightness Temperatures (Stewart et al., 2025) data set created by NSIDC as input to CDR V6. NSIDC created it specifically to match SSMIS 25 km gridded brightness temperatures, following the steps below. Further processing information can be found in the user guide for that product (Table 3), but it is summarized here for easy reference.

1. Retrieve reduced-resolution AMSR2 L1R brightness temperature swath data from JAXA. These better match the SSMIS sensor resolution (IFOV). See Table 2 for a list of IFOVs by sensor.

2. Grid the L1R swath brightness temperatures onto the NSIDC 25 km polar stereo grid using the drop-in-the-bucket method (simple sum-and-average).

3. Perform a one-time linear regression on the gridded brightness temperatures during an AMSR2 and SSMIS overlap for each channel for the year 2017 (2024 for 37H channel). Separate slope and offset coefficients were calculated for each channel.

4. Apply the resulting regression coefficients (slope and intercept) to AMSR2 brightness temperature time series to make them more consistent with SSMIS.

5. Apply a Gaussian-smoothing filter to improve spatial matching for each channel. Separate Gaussian-filter coefficients were calculated for each channel.

While these procedures cannot fully compensate for the differences in sensor and orbit between the SSMIS and AMSR2 data sources, they do provide fields which can be incorporated into sea ice concentration algorithms designed for SSMIS 25 km gridded data.

Sensor	**Temporal Coverage Range**	**CDR Product**	**Input Brightness Temperature Product**
GCOM-W1 AMSR2	Near-real-time	ICDR (G10016 V4)	AMSR2 Daily Polar Gridded Brightness Temperatures* (Stewart et al., 2025) (https://nsidc.org/data/nsidc-0802)
GCOM-W1 AMSR2	01 Jan 2025 – most recent processing	TCDR (G02202 V6)	AMSR2 Daily Polar Gridded Brightness Temperatures* (Stewart et al., 2025) (https://nsidc.org/data/nsidc-0802)

DMSP-F17 SSMIS	01 Jan 2008 – 31 December 2024	TCDR (G02202 V6)	DMSP SSM/I-SSMIS Daily Polar Gridded Brightness Temperatures (Meier et al., 2021) (https://nsidc.org/data/nsidc-0001)
DMSP-F13 SSM/I	01 Oct 1995 – 31 December 2007	TCDR (G02202 V6)	DMSP SSM/I-SSMIS Daily Polar Gridded Brightness Temperatures (Meier et al., 2021) (https://nsidc.org/data/nsidc-0001)
DMSP-F11 SMM/I	03 Dec 1991 – 30 Sep 1995	TCDR (G02202 V6)	DMSP SSM/I-SSMIS Daily Polar Gridded Brightness Temperatures (Meier et al., 2021) (https://nsidc.org/data/nsidc-0001)
DMSP-F8 SSM/I	10 Jul 1987 – 02 Dec 1991 Note: There are no data from 3 December 1987 through 13 January 1988 due to satellite problems.	TCDR (G02202 V6)	DMSP SSM/I-SSMIS Daily Polar Gridded Brightness Temperatures (Meier et al., 2021) (https://nsidc.org/data/nsidc-0001)
Nimbus-7 SMMR	25 October 1978 – 09 Jul 1987	TCDR (G02202 V6)	Nimbus-7 SMMR Polar Gridded Radiances and Sea Ice Concentrations (Gloersen, 2006) (https://nsidc.org/data/nsidc-0007)

Table 3: Temporal coverage range of the instruments used for the input brightness temperatures used in each data product. *The AMSR2 product contains a calibrated and uncalibrated version. The calibrated version is used in CDR V6, which is calibrated using the five steps listed above this table.

NSIDC grids the SMMR, SSM/I, SSMIS, and AMSR2 swath brightness temperature data onto a daily composite 25 km polar stereographic grids (one for northern hemisphere and one for southern) using a drop-in-the-bucket method to produce the data sets listed in Table 3. For each grid cell, all footprints from every pass for a given day whose centers fall within the grid cell are averaged together. Thus, some grid cells may be an average of up to five passes during a given day and some may be from only one pass.

Note that the Northern and Southern Hemisphere polar stereographic grids are not equal area; the latitude of the true scale (tangent of the planar grid) is 70° N and 70° S, respectively. The Northern Hemisphere grid is 304 columns by 448 rows, and the Southern Hemisphere grid is 316 columns by 332 rows. More information about the grid can be found in the Guide to NSIDC's Polar Stereographic Projection (https://nsidc.org/data/user-resources/help-center/guide-nsidcs-polar-stereographic-projection).

The passive microwave channels employed for the sea ice concentration product are the 19 GHz (V/H), 22 GHz (V), and 37 GHz (V/H) frequencies. The NASA Team algorithm uses the 19 GHz (V/H) channels and the 37 GHz V channel. The 22 GHz V channel is used with the 19 GHz V channel for one of the weather filters. The Bootstrap algorithm uses 37 GHz (V/H) channels and the 19 GHz V channel; it also uses the 22 GHz V channel for a weather filter.

3.3.2 Ancillary Data

Ancillary data required to run the CDR SIC processing are: (A) surface type mask, (B) invalid sea ice masks, (C) land adjacency mask, (D) land-90%-concentration mask, and (E) Arctic pole hole mask. These are described briefly below and are discussed further in Section 3.4.1.4. Section 5.5.1 describes the files that contain these ancillary data.

A. The surface type mask provides a mask of these surface types: ocean, lake, coast, and land.

B. Invalid sea ice masks define the geographic boundaries of possible sea ice formation and are used to remove any spurious or questionable ice in regions where sea ice is not likely possible. This reduces the inclusion of clearly false-positive ice concentration values. There are masks for each hemisphere, one for each month. In addition, for the noisier SMMR era data, there are daily climatology ice masks derived from Bootstrap Sea Ice Concentrations (Comiso, 2023) for both the Northern and Southern hemispheres. Ocean cells that are not valid sea ice locations are set to 0% concentration.

C. The land adjacency mask is a mask that indicates whether ocean grid cells are 1, 2, 3, or >3 pixels away from land. This is used for the Bootstrap (BT) and NASA Team 2 (NT2) land-spillover correction algorithms.

D. The land-90%-concentration mask is a mask that estimates how land might look if it was interpreted as sea ice. Along with the land adjacency mask (C), it is used by the NT2 land-spillover algorithm to automatically remove false coastal ice grid cells. This estimate is calculated by assuming that nearby ocean grid cells are 0% sea ice concentration and nearby land grid cells are 90% sea ice concentration and computing the average of grid cells near each point. The idea is to know what sea ice concentration value a grid cell would have if it were close enough to land to be affected by land spillover even if there is no sea ice there. If we know this value in advance, and the calculated sea ice concentration is greater than that, then it is likely that there really is ice there.

E. The Arctic pole hole masks define where observations are not possible because satellite swaths do not reach that far north. A pole hole mask file has been generated for each sensor so that these unobserved locations can be treated differently than other missing data. Table 4 lists the sizes of these holes. In this data product, the pole hole is filled where possible.

Sensor	Arctic Pole Hole Area (x 10^6 km^2)	Minimum Latitude
SMMR	1.193	84.12° N
SSM/I F08	0.318	86.72° N
SSM/I F11	0.318	86.72° N
SSM/I F13	0.318	86.72° N
SSMIS F17	0.0292	89.02° N
AMSR2*	0.064	88.5° N

Table 4. Arctic Pole Hole Sizes by Instrument.
*Due to the use of the AMSR2 L1R data, the pole hole is slightly larger than the SSMIS pole hole.

3.4 Theoretical Description

Passive microwave radiation is naturally emitted by the Earth's surface and overlying atmosphere. This emission is a complex function of the microwave radiative properties of the emitting body (Hallikainen and Winebrenner, 1992). However, for the purposes of microwave remote sensing, the relationship can be described as a simple function of the physical temperature (T) of the emitting body and the emissivity (ε) of the body,

$$T_B = \varepsilon * T \quad (8)$$

where T_B, or brightness temperature, is the parameter (after calibrations) retrieved by satellite sensors and is the input parameter to passive microwave sea ice concentration algorithms.

3.4.1 Physical and Mathematical Description

The microwave electromagnetic properties of sea ice are a function of the physical properties of the ice, such as crystal structure, salinity, temperature, and snow cover. Open water typically has an electromagnetic emission signature that is distinct from sea ice emission (Eppler et al., 1992). These properties form the basis for passive microwave retrieval of sea ice concentrations.

Specifically, the unfrozen water surface is highly reflective in much of the microwave regime, resulting in low emission. In addition, emission from liquid water is highly polarized. When salt water initially freezes into first-year (FY) ice (ice that has formed since the end of the previous melt season), the microwave emission changes substantially; the surface emission increases and is only weakly polarized. Over time as freezing continues, brine pockets within the sea ice drain, particularly if the sea ice survives a summer melt season when much of the brine is flushed by melt water. This multiyear (MY) ice has a more complex signature with characteristics generally between water and FY ice. Other surface features can modify the microwave emission, particularly snow cover, which can scatter the ice surface emission and/or emit radiation

from within the snowpack. Atmospheric emission also contributes to any signal received by a satellite sensor. These issues result in uncertainties in the retrieved concentrations, discussed below.

Because of the complexities of the sea ice surface as well as surface and atmospheric emission and scattering, direct physical relationships between microwave emission and sea ice concentration are not feasible. Thus, the standard approach is to derive concentration through empirical relationships. These empirically-derived algorithms take advantage of the fact that brightness temperature in microwave frequencies tend to cluster around consistent values for pure surface types (100% water or 100% sea ice). Concentration can then be derived using a simple linear mixing equation (Zwally et al., 1983) for any brightness temperature that falls between the two pure surface values:

$$T_B = T_I C_I + T_O(1-C_I) \quad (9)$$

where T_B is the observed brightness temperature, T_I is the brightness temperature for 100% sea ice, T_O is the brightness temperature for open water, and C_I is the sea ice concentration.

In practice, such an approach is limited by the surface ambiguities and atmospheric emission. Using combinations of more than one frequency and polarization limits these effects, resulting in better discrimination between water and different ice types and a more accurate concentration estimate.

There have been numerous algorithms derived using various combinations of the frequencies and polarizations on the SMMR and SSM/I sensors. Two commonly used algorithms are the NASA Team (Cavalieri et al., 1984) and Bootstrap (Comiso, 1986), both developed at NASA GSFC. The sea ice concentration CDR described here is produced via a combination of estimates from the NASA Team algorithm and the Bootstrap algorithm. Below, each algorithm is described in more detail followed by a description of quality control (QC) procedures and the method to merge the two algorithm estimates into the final CDR product with the sea ice concentration CDR algorithm.

While the NASA Team and Bootstrap algorithms were originally designed for SMMR and SSM/I, they are also compatible with newer sensors such as SSMIS and AMSR2 because these have similar channel frequencies as the older sensors.

3.4.1.1 NASA Team Algorithm

The NASA Team algorithm uses brightness temperatures from the 19V, 19H, and 37V channels (Cavalieri et al., 1984). The methodology is based on two brightness temperature ratios, the polarization ratio (PR) and spectral gradient ratio (GR), as defined below:

$$PR(19) = [T_B(19V) - T_B(19H))]/[T_B(19V) + T_B(19H)] \quad (10)$$

$$GR(37V/19V) = [T_B(37V) - T_B(19V)]/[T_B(37V) + T_B(19V)] \quad (11)$$

When PR and GR are plotted against each other, brightness temperature values tend to cluster in two locations, an open water (0% ice) point and a line representing 100% ice concentration, roughly forming a triangle. The concentration of a grid cell with a given GR and PR value is calculated by a linear interpolation between the open water point and the 100%-line segment (Figure 6).

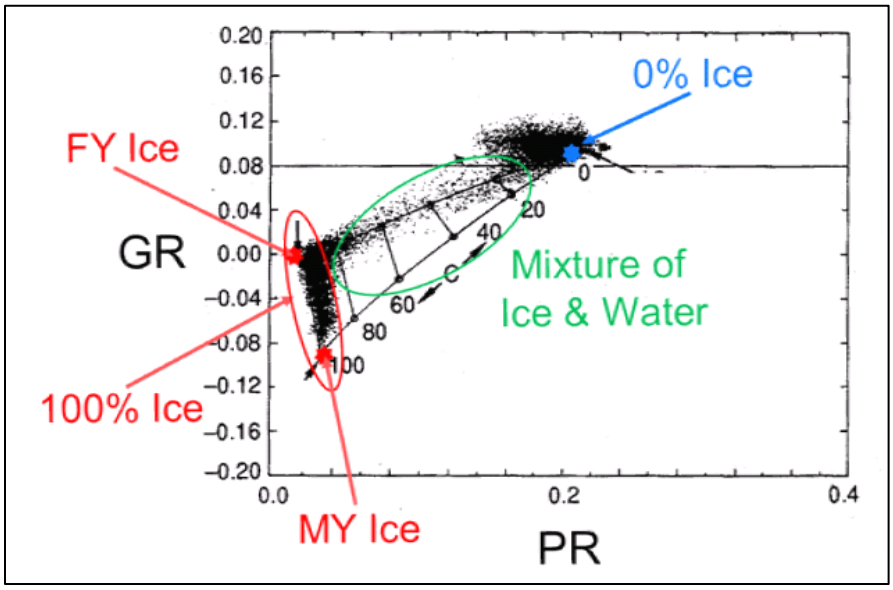

Figure 6: Sample plot of GR vs. PR with typical clustering of grid cell values (small black dots) around the 0% ice (open water) point (blue star) and the 100% ice line (circled in red). First-year (FY) ice clusters at the top of the 100% ice line, and multiyear (MY) ice clusters at the bottom. Points with a mixture of ice and water (circled in green) fall between these two extremes. Adapted from Figure 10-2 of Steffen et al. (1992).

Mathematically, these two ratios are combined in the following two equations:

$$C_F = (a_0 + a_1PR + a_2GR + a_3PR * GR)/D \quad (12)$$

$$C_M = (b_0 + b_1PR + b_2GR + b_3PR * GR)/D \quad (13)$$

$$where\ D = c_0 + c_1PR + c_2GR + c_3PR * GR \quad (14)$$

The C_F and C_M parameters represent ice concentration for two different sea ice types. In the Arctic, these generally correspond to FY ice (C_F: ice that has grown since the previous summer) and MY ice (C_M: ice that has survived at least one melt season). In the Antarctic, due to its small amount of MY ice and different ice characteristics, C_M and C_F do not necessarily correspond to the age types and are simply denoted as Type A and Type B. Total ice concentration (C_T) is the sum of the two partial concentrations.

$$C_T = C_F + C_M \quad (15)$$

The a_i, b_i, c_i (i=0, 3) coefficients are empirically derived from nine observed brightness temperatures at each of the 3 channels for 3 pure surface types (two sea ice and one open water). These brightness temperatures, called tie-points, are represented in Figure 6 by the points for 100% MY ice, 100% FY ice, and 0% ice. They were originally derived for the SMMR sensor (Cavalieri et al., 1984). Cavalieri et al. (1999) devised a method to ensure consistency through the time series by adjusting for subsequent sensors via intercalibration of the concentration and extent fields during sensor overlap periods. Section 3.4.2 has more information on how this is done.

Table 5 lists the tie-points for all sensors.

NIMBUS 7 SMMR				
Arctic		**18H**	**18V**	**37V**
	OW	98.5	168.7	199.4
	FY	225.2	242.2	239.8
	MY	186.8	210.2	180.8
Antarctic				
	OW	98.5	168.7	199.4
	A	232.2	247.1	245.5
	B	205.2	237.0	210.0
DMSP-F8 SSMI				
Arctic		**19H**	**19V**	**37V**
	OW	113.2	183.4	204.0
	FY	235.5	251.5	242.0
	MY	198.5	222.1	184.2
Antarctic				
	OW	117.0	185.3	207.1
	A	242.6	256.6	248.1
	B	215.7	246.9	212.4
DMSP-F11 SSMI				
Arctic		**19H**	**19V**	**37V**
	OW	113.6	185.1	204.8
	FY	235.3	251.4	242.0
	MY	198.3	222.5	185.1
Antarctic				
	OW	115.7	186.2 -0.4	207.1
	A	241.2	255.5	245.6
	B	214.6	246.2	211.3
DMSP-F13 SSMI				

Arctic		**19H**	**19V**	**37V**
	OW	114.4	185.2	205.2
	FY	235.4	251.2	241.1
	MY	198.6	222.4	186.2
Antarctic				
	OW	117.0	186.0	206.9
	A	241.4	256.0	245.6
	B	214.9	246.6	211.1
DMSP-F17 SSMIS				
Arctic		**19H**	**19V**	**37V**
	OW	113.4	184.9	207.1
	FY	232.0	248.4	242.3
	MY	196.0	220.7	188.5
Antarctic				
	OW	113.4	184.9	207.1
	A	237.8	253.1	246.6
	B	211.9	244.0	212.6
AMSR2 L1R				
Arctic		**19H**	**19V**	**37V**
	OW	120.50	185.90	210.50
	FY	235.50	250.90	241.30
	MY	200.70	222.20	188.60
Antarctic				
	OW	118.20	192.40	208.70
	A	240.90	256.40	246.20
	B	214.60	246.70	212.40

Table 5: NASA Team tie-point values (in Kelvin) for each sensor.

Note that the NASA Team algorithm can sometimes calculate concentration values that are greater than 100%, which is clearly unphysical. Once these have been passed through the CDR algorithm, such values are set to 100%.

3.4.1.2 Bootstrap Algorithm

Like the NASA Team algorithm, the Bootstrap algorithm is empirically derived based on relationships of brightness temperatures at different channels. We use the current version of the Bootstrap algorithm, 3.1 (Comiso et al., 2017), in CDR processing. The Bootstrap method uses the fact that scatter plots of different sets of channels show

distinct clusters that correspond to pure surface types (100% sea ice or open water) (Comiso, 1986).

The scatterplots in Figure 7 show the general relationship between brightness temperatures from 37V versus 19V (left) and 37V versus 37H (right). Points that fall along line segment AD represent 100% ice cover. Points that cluster near point O represent open water (0% ice). Within the pack, away from the ice edge, the algorithm uses the relationship between 37V and 37H brightness temperatures. Concentration for a point B is determined by a linear interpolation along the distance from O to I where I is the intersection of segment OB and segment AD. In the example shown Figure 7 (right), point B is about halfway between I and O, and it represents a grid cell with about 50% SIC.

Grid cells that are well within the pack will have a 19V brightness temperature that is within 5 K of the 19V temperature represented by the AD line in the 37V vs 19V plot in Figure 7 (left). Near the ice edge, grid cells do not meet this criterion. For these, the 37V and 19V channels are used to derive the concentration values following the same method as that illustrated in Figure 7 (right). The 37V and 19V combination is more sensitive to the ice-water boundary, making it a better choice for discriminating concentrations that define this boundary.

This is described by the following equation:

$$C = (T_B - T_O)/(T_I - T_O) \qquad (16)$$

where T_B is the observed brightness temperature, T_I is the brightness temperature for 100% sea ice, T_O is the brightness temperature for open water, and C is the sea ice concentration.

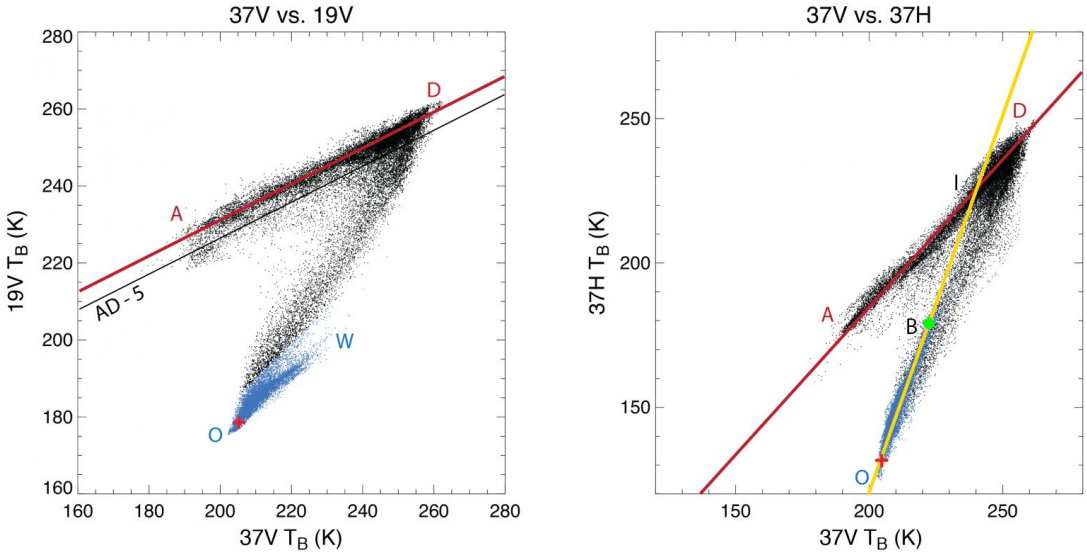

Figure 7: Example of the relationship between brightness temperatures for 37V vs. 19V (left) and 37V vs. 37H (right). In both, blue points are open water. Brightness temperatures

typically cluster around the line segments AD (representing 100% sea ice) and OW (representing 100% open water). Adapted from Comiso and Nishio (2008).

Slope and offset values for line segment AD were originally derived for each hemisphere for different seasonal conditions (Table 2 in Comiso et al, 1997). In a later formulation, slope and offsets are derived for each daily field based on the clustering of sea ice signatures within the daily brightness temperatures (Comiso and Nishio, 2008). This dynamic tie-point adjustment allows for day-to-day changes in sea ice microwave characteristics. Comiso et al. (2017) refined the algorithm, including adjusting open water tie-points. It is this latest version of the Bootstrap algorithm (version 3.1), with dynamic sea ice and open water tie-points, that is used in version 6 of the CDR. Section 3.4.2 has more information on how these tie-points are calculated.

The Bootstrap algorithm can sometimes calculate concentration values that are greater than 100%, which is clearly unphysical. Once these have been passed through the CDR algorithm, such values are set to 100%.

3.4.1.3 Sea Ice Concentration Climate Data Record Algorithm

NSIDC processes the daily input brightness temperatures into two intermediate sea ice concentrations using the two NASA GSFC-developed algorithms: NASA Team (Cavalieri et al., 1984) and Bootstrap (Comiso, 1986) described above in sections 3.4.1.1 and 3.4.1.2, respectively. Then, these two intermediate sea ice concentrations are merged using the sea ice concentration CDR algorithm described below.

The NASA Team and Bootstrap algorithms are run independently to create raw NT and BT sea ice concentrations (i.e. no filters have been applied). Then, the concentration values from both are merged to create the CDR ice concentration field based on the steps defined below. Finally, automated quality control filters are applied.

1. Sea ice concentrations estimated by the Bootstrap algorithm are analyzed. A 10% concentration threshold is used to define valid ice – any grid cell with a Bootstrap concentration of less than 10% is set to 0%. A 15% cutoff is a common standard that has been in use for many years (Zwally et al., 1983); and in comparisons with other satellite data, has agreed well, on an average basis, with the observed ice (Cavalieri et al., 1991; Meier et al., 2003). Further, the applied weather filters typically remove most concentrations below 15% (Cavalier et al., 1999). However, there are indications that the Bootstrap algorithm can potentially detect ice as low as 8% concentration (Comiso and Nishio, 2008). To be conservative, we chose a 10% cutoff for the CDR data fields. The validity of the assumption that ice concentrations greater than 10% and less than 15% are good data depends on ocean and atmospheric conditions; and, for grid cells near open water, on the condition of the ice edge. We recommend that users deriving total extent and area calculations continue to use a 15% cutoff. Even a relatively low 10% cutoff in the CDR field will miss some real ice, but low concentrations have much higher uncertainties. The 10% cutoff removes many potentially high-

error concentration estimates and provides a standard throughout the time series.

2. At each sea ice grid cell, the concentration of the NASA Team and the Bootstrap output are compared, and whichever value is greater is selected as the CDR value. This is because both algorithms tend to underestimate concentration, and the one that gives the higher concentration value is assumed to be more correct. In most cases, it is the Bootstrap algorithm. Generally speaking, NASA Team concentrations tend to have a larger low bias than those from Bootstrap (Kwok, 2002; Meier, 2005). During melt conditions, both algorithms tend to underestimate concentration; but the effect is more pronounced in the NASA Team algorithm (Comiso et al., 1997; Meier, 2005; Andersen et. al, 2007). However, the Bootstrap algorithm uses relationships between two brightness temperatures that are dependent on physical temperature. Thus, physical temperature changes can affect Bootstrap estimates. This occurs primarily in regimes with very low temperatures: winter in the high Arctic and near the Antarctic coast (Comiso et al., 1997), where low temperatures can result in concentration values that are biased lower than NASA Team results.

   The NASA Team algorithm, because it uses a ratio of brightness temperatures, tends to cancel out any physical temperature effects, and concentration values are not affected by low temperature regimes.

   While these characteristics of the contributing algorithms are realistic in a general sense, ice conditions and algorithm performance can vary from grid cell to grid cell; and in some cases, this approach will result in an overestimation of concentration (Meier, 2005). However, using the higher concentration between the two algorithms will tend to reduce the overall underestimation of the CDR estimate. These details are discussed Section 4.2.3.

The final CDR concentration field grid cells are therefore a combination of grid cells with values that came from the NASA Team algorithm and grid cell with values from the Bootstrap algorithm. Detected ice grid cells may have concentration values between 10% and 100%.

The monthly average is computed at each grid cell by averaging all available daily quality-controlled values in the month for that grid cell. A minimum of 20 days (10 for SMMR) is required for a valid monthly value. If a grid cell has fewer than 20 days of data, that grid cell is assigned the missing flag in the monthly field. Monthly concentration values of less than 10% may occur because the average of a grid cell for a month may be lower but these concentrations are set to zero to maintain the 10% threshold.

3.4.1.4 Quality Control Procedures

Several automated quality control procedures improve the quality of the data product. These include filling missing data (gap filling) and filtering out spurious ice concentration values.

3.4.1.4.1 Gap Filling

Small amounts of missing data are common in satellite data, especially over a satellite record spanning more than 40 years. Reasons for missing data are numerous and range from issues with the instrument onboard the satellite, satellite viewing angles, and problems arising at the ground stations when data are downloaded from the satellite. These missing data are handled in several ways in the CDR processing code. First, a spatial interpolation is performed on the input brightness temperature data to fill small gaps (a few pixels). Then, temporal interpolation is performed on the sea ice concentration data to fill larger gaps (full swaths or entire days). Finally, in the Arctic where an area of missing pixels called the pole hole exists, missing grid cells are filled from a sea ice concentration average. These automated gap filling methods are described in further detail in the sections below.

Brightness Temperature Spatial Interpolation

The input brightness temperatures that are used to produce the sea ice CDR sometimes contain small gaps in the data fields. These occur commonly in the fields, especially in the more equator-ward parts of the grids. This is because of the drop-in-the-bucket method used for gridding the brightness temperature swath data. This method simply averages all footprints (swaths) into a grid for a given day based on the center location of the footprint. For example, at each grid cell, all footprints whose centers are within that grid cell's boundaries are found. However, because the footprints are larger than the grid cell size, some grid cells have no footprint centers. Thus, these are empty grid cells (i.e., have a missing or zero value). These happen more equator-ward because there are fewer overlapping swaths and thus more chance of empty grid cells.

These empty grid cells are generally isolated, that is, 1 or 2 missing grid cells surrounded by cells with valid brightness temperature values. To correct these missing grid cells, the SIC CDR code fills them by bilinear interpolation where the grid cell is filled with the weighted average of the eight grid cells that surround it: one above, one below, one to the left, one to the right, and the four diagonal grid cells. The orthogonal neighbors are weighted with 1.0 and the diagonal neighbors are weighted with 0.707. To make the spatial gap filling algorithm more widely applicable in cases where more than 1 missing grid cell occurs in a location, a total weighting threshold of at least 1.2 is required. This means that at least two out of the eight surrounding cells must contain valid brightness temperature values for the interpolation to proceed. A flag called cdr_seaice_conc_interp_spatial_flag marks the grid cells that were interpolated. See Section 3.4.4.1 for more information on this flag.

This spatial interpolation is performed on all channels prior to the input data being passed into the CDR sea ice concentration algorithms. Larger gaps in the data, such as entire swaths or days, are filled by temporal interpolation (see the next section below).

Sea Ice Concentration Temporal Interpolation

To fill larger gaps in the data such as missing swaths or full missing days of data, a temporal linear interpolation is performed on the sea ice concentration data. Once the brightness temperatures are processed through the CDR sea ice algorithm, the temporal interpolation is applied. The method of interpolation is performed by locating a missing sea ice concentration grid cell on a particular date and then using linear interpolation to fill that value from data on either side of that date. Data can be interpolated with values of up to five days on either side of the missing date and those days do not have to be evenly spaced on either side. For example, a missing grid cell can be interpolated from data from a corresponding grid cell one day in the past and one day in the future or two days in the past and four days in the future, up to five days in the past and five days in the future. The interpolation is weighted, whereby data closer to the missing date (e.g. 1 day away) are given more weight than data further away (e.g. 5 days away). This linear interpolation method is the preferred technique of temporal interpolation. However, in some cases, gaps still exist after this interpolation scheme is performed because two data points on either side of the missing value are not found. To attempt to further fill these gaps, a single-sided gap filling is performed where the code checks if there is at least one data value up to three days on either side of the date and then simply copies that single value into the missing grid cell. A flag called cdr_seaice_conc_interp_temporal_flag marks the data that were interpolated. See Section 3.4.4.1 for more information on this flag.

Pole Hole Spatial Interpolation

A polar orbit and wide swath provide near-complete coverage at least once per day in the polar regions except for a small region around the North Pole called the pole hole. The size of this hole has changed over time as the instruments have become more advanced. See Table 4 for a list of the sizes of the holes by instrument.

To provide a sea ice concentration grid with complete geographic coverage, the pole hole is filled with an average of the sea ice concentrations from the grid cells that surround the hole. Note that this method means that all grid cells within the pole hole have the same concentration value. The cdr_seaice_conc_interp_spatial_flag variable identifies this region. See Section 3.4.4.1 for more information on this flag.

Note: The current pole hole is quite small (Table 4); and even though the sea ice edge has retreated a great deal in recent years, the hole is still within the boundary of where ice is likely to exist. However, this could change, and one cannot assume what the concentration is, especially in late Arctic summer and early autumn. Thus, we would advise caution in using the interpolated data in long-term trends or climatology analyses and would generally recommend against it. Users should apply the pole hole mask before making a time series analysis (see Section 5.5.1.1).

3.4.1.4.2 CDR Sea Ice Filtering

False or questionable ice retrievals can occur from passive microwave data. The main sources of the spurious ice grid cells are ocean surface brightness temperature variation, atmospheric emission from weather, and mixed land-ocean IFOV (known as land spillover) in a grid cell. To contend with false ice from weather effects, two weather filters are applied: the NASA Team weather filter and the Bootstrap weather filter. To remove false ice from land spillover, two land-spillover algorithms are employed: the NASA Team 2 land spillover and the Bootstrap land spillover. As a further step, monthly climatological invalid ice masks are applied that remove ice where it would not naturally occur. While these filters and masks are tuned to be as accurate as possible, it is possible that they may remove real ice in some conditions or leave false ice behind. These methods are described in the sections below.

Weather Filters

Weather effects can cause the passive microwave signature of seawater to appear like that of ice (Cavalieri et al., 1995). Both The NASA Team and Bootstrap sea ice algorithms assume that open water can be represented as a single point in the clustering of different channel combinations. However, Figure 6 and Figure 7 suggest that there is significant spread around the open water point. This is primarily due to weather effects, namely: roughening of the ocean surface by winds, which increases the microwave emission of the water; and atmospheric emission, primarily due to water vapor and liquid water (as in clouds), which will also increase the emission retrieved by the sensor. Atmospheric emission is most pronounced during rainfall over the open ocean. Emission from the atmosphere has the largest effect on the 19 GHz channels because they are near to frequencies in which there is strong water vapor emission.

Most of these false-ice signatures are removed with a standard brightness-temperature filter, but some are too close to those of real ice and require another method to be removed. Unlike sea ice products produced at NASA GSFC, which have manual corrections applied, the NSIDC SIC CDR uses an automated process to filter any lingering false ice. This is accomplished by applying the following filters to the CDR sea ice concentrations: the NASA Team weather filter and the Bootstrap weather filter. This takes the place of the GSFC manual corrections. Although it may not remove all false ice as well as manual correction can, it is a good approximation and is fully traceable.

- *NASA Team Weather Filters*

Spurious ice over open water is removed by a threshold of the GR3719 ratio (Equation 9) and an additional GR2219 ratio:

$$GR(22V/19V) = [T_B(22V) - T_B(19V)]/[T_B(22V) + T_B(19V)] \quad (17)$$

using the criteria listed in Table 6 (Cavalieri et al., 1995).

Instrument	Hemisphere	Criteria
SMMR	Northern	GR3719 > 0.070 → concentration = 0 GR2219 → N/A
SMMR	Southern	GR3719 > 0.076 → concentration = 0 GR2219 → N/A
SSM/I	Northern	GR3719 > 0.050 → concentration = 0 GR2219 > 0.045 → concentration = 0
SSM/I	Southern	GR3719 > 0.050 → concentration = 0 GR2219 > 0.045 → concentration = 0
SSMIS	Northern	GR3719 > 0.050 → concentration = 0 GR2219 > 0.045 → concentration = 0
SSMIS	Southern	GR3719 > 0.057 → concentration = 0 GR2219 > 0.045 → concentration = 0
AMSR2	Northern	GR3719 > 0.050 → concentration = 0 GR2219 > 0.045 → concentration = 0
AMSR2	Southern	GR3719 > 0.057 → concentration = 0 GR2219 > 0.045 → concentration = 0

Table 6. GR3719 and Gr2219 criteria by instrument and hemisphere

- *Bootstrap Weather Filters*

The Bootstrap algorithm also uses combinations of 19V, 22V, and 37V as weather filters, and the methodology follows the overall Bootstrap by thresholding above a cluster of points in (1) 19V vs. 37V, and (2) 19V vs. (22V-19V) brightness temperature scatter plots (Figure 8) (Comiso and Nishio, 2008; Cho and Naoki, 2023).

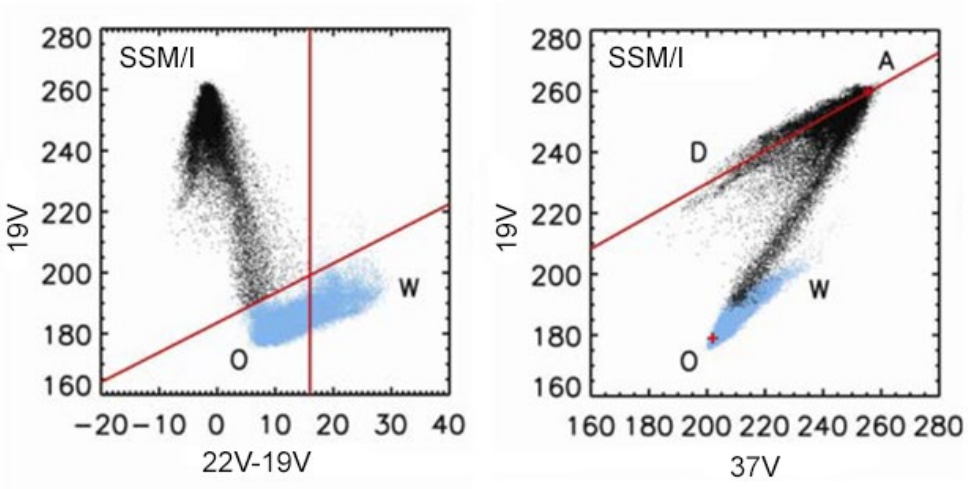

Figure 8: Sample scatter plot of 19V vs. (22V-19V) (left) and 19V vs. 37V (right) TBs from SSM/I. Values shaded in blue around the OW segment are masked to 0% concentration. From Comiso and Nishio (2008).

Land-Spillover Corrections

Spurious ice is common along ice-free coasts. Because of the large IFOV (up to 72 km x 44 km for the 19 GHz channel on SSMIS), brightness temperature values from ocean grid cells near the coast often contain microwave emission from both land and ocean. These mixed grid cells of ocean/land have a brightness temperature signature that is often interpreted by the algorithms as sea ice. When sea ice is actually present along the coast, the effect is small, but when there is no ice present, artifacts of false ice appear. This is commonly called the land-spillover effect because emission from the land surface “spills over” into ocean grid cells. To correct for this land spillover, the SIC CDR algorithm uses two automated land-spillover corrections: NASA Team 2 and Bootstrap. They are described below.

- *NASA Team 2 Land-Spillover Correction*

The NASA Team 2 (NT2) land-spillover correction is a data filtering mechanism to automatically identify and correct many of these false-coastal-ice grid cells. The NT2 land-spillover consists of two checks to determine if apparent sea ice is likely to be a misclassification due to nearby land inside the passive microwave sensor's field of view. These are briefly described below. For a full explanation of the NT2 methodology, see Markus and Cavalieri (2009).

1. The algorithm will assume that sea ice along the coast will extend out to at least three grid cells away from land. A land adjacency mask is used to identify these grid cells; it is described in Section 3.3.2. Grid cells that are one or two grid cells from land are considered near-coast and grid cells further away are considered away-from-coast. If a near-coast grid cell does not have any away-from-coast grid cells with at least 50% sea ice concentration within a 7x7 grid cell matrix centered on itself, the near-coast grid cell's concentration is assumed to be false and is set to zero.

2. It is probable that near-coast grid cells will have an apparent sea ice concentration because land appears similar to sea ice at the passive microwave frequencies used in the sea ice concentration calculation. Land pixels are assumed to have an ice concentration of 90%, which is an estimate of the sea ice concentration that the algorithm might be expected to compute simply from the presence of nearby land. A 90% concentration land mask is used in the calculation of this step; it is described in Section 3.3.2. If the calculated sea ice concentration of a near-coast grid cell is less than this value, it is considered false ice and set to zero.

- *Bootstrap Land-Spillover Correction*

The Bootstrap land-spillover algorithm expects that estimated sea ice that is only found within a grid cell or two of land is likely to be a result of the land within the sensor's field of view. If no sea ice is detected in nearby far-from-land grid cells, the sea ice

concentration of near-land grid cells is assumed to be false and set to zero (Comiso, 2009).

Invalid Ice Masks

As noted in the sections above, false ice can occur from weather effects and land-spillover. While weather filters and land-spillover corrections remove much of this false ice, some can remain. Applying an invalid ice mask can help to remove any lingering false ice. There are different invalid ice masks used for each hemisphere; they are described below.

- *Northern Hemisphere*

The best way to evaluate where ice can be is to look at a climatology of sea ice occurrence, where the climatology is built from Arctic-wide sea ice analyses over as long a period as possible from many different sources. These show where ice detected by the satellite data algorithm is most likely to be valid ice, based on where ice has existed in the past.

For the Northern Hemisphere, any remaining weather effects and land spillover are corrected with valid ice masks from the *Polar Stereographic Valid Ice Masks Derived from National Ice Center Monthly Sea Ice Climatologies* data product available from NSIDC (Meier et al., 2015). The climatology used for these masks is the *U.S. National Ice Center Arctic Sea Ice Charts and Climatologies in Gridded Format, 1972 - 2007* (U.S. National Ice Center, 2006). The valid ice masks include 12 masks showing the maximum sea ice extent, one for each month of the year, over the period 1972 to 2007. An additional mask is applied only to the SMMR era data due to the poor quality of these older data.

This mask is a day-of-year climatology ice mask that is derived from the GSFC Bootstrap sea ice concentrations data set (Comiso, 2023) – a manually quality controlled sea ice concentration estimate. NSIDC developed this mask specifically for the ice concentration CDR. We create the day-of-year sea ice climatology by reviewing the Comiso (2023) data record of sea ice concentration for November 1978 through December 2023 and noting every time sea ice existed within plus/minus four days of each day of year. This gives us a conservative estimate of whether sea ice has ever been detected within about a week of each day-of-year at each cell in our grids. For example, if sea ice exists in a grid cell on January 3 of a year, we indicate that sea ice is possible from December 30 to January 7.

- *Southern Hemisphere*

In the Southern Hemisphere, masks based on the monthly sea surface temperature (SST) climatology of Levitus and Boyer (1994) are used to remove remaining false ice. A temperature threshold of 275 K was used to determine the mask boundary for each month. Any sea ice concentrations above 0% calculated by the algorithms in regions where the masks do not allow sea ice are set to zero in the final concentration

estimates. An additional mask is applied only to the SMMR era data due to the poor quality of the older data. For a description of this mask, see the Invalid Ice Masks Northern Hemisphere section above.

3.4.2 Intercalibrating Between Sensors with Tie-Points

As noted in sections 3.4.1.1 and 3.4.1.2, both the NASA Team and Bootstrap algorithms use platform- and channel-dependent tie-points to account for changes in sensors and spacecraft. These tie-point adjustments are derived from regressions of brightness temperatures during instrument overlap periods. The adjustments are made at the product level by adjusting the algorithm coefficients so that the derived sea ice fields are as consistent as possible.

There are several reasons to adopt this approach. First, NASA Team and Bootstrap algorithms use daily mean gridded brightness temperatures that have been made from swath data with a simple drop-in-the-bucket average for each grid cell. Each sun-synchronous sensor has a different equatorial crossing time. This means that during an overlap period, the gridded brightness temperature for a given grid cell will be comprised of swath brightness temperature values from different times of day coming from the old sensor and the new sensor. Because sea ice, as well as the overlying atmosphere, varies over time, this will result in inconsistencies in the brightness temperature signal for a particular grid cell location. Second, sea ice varies on spatial scales far smaller than the footprint of the passive microwave sensors. Thus, any retrieved brightness temperature is likely a mixture of several different surfaces (for example, first-year and multiyear, smooth and rough/ridged, deep snow and snow free, etc.). This makes it difficult to directly match up brightness temperatures from different sensors to the same sea ice conditions for the purposes of intercalibration. Finally, transitions between sensors may result in a change of frequency. Notably, this occurs for the SMMR to SSM/I transition, where the 18.0 GHz channel on SMMR was replaced by a 19.4 GHz channel on SSM/I. There are also small differences in frequencies between SSMIS and AMSR2 (see Table 2).

The NASA Team and Bootstrap algorithms approach intercalibrating sea ice concentration using tie-points differently. The next two sections describe this.

3.4.2.1 NASA Team Tie-Points

The NASA Team approach uses sensor-specific hemispheric tie-points for each transition (Cavalieri et al., 1999; Cavalieri et al., 2011). Cavalieri et al. (1999) originally derived the NASA Team tie-points for the SMMR sensor. For subsequent transitions to SSM/I and SSMIS, they adjusted the tie-points to be consistent with the original SMMR record. This work was done at NASA GSFC.

Tie-point adjustments are made via a linear regression analysis along with additional adjustments for open water tie-points. The tie-point adjustment procedure and tie-point values for all SMMR and SSM/I sensors are provided in Cavalieri et al. (1999). Tie-

points for SSMIS are described in Cavalieri et al. (2011). These Cavalieri-produced NASA Team tie-points used in CDR V6 are listed in Table 5.

NASA Team tie-points had not been calculated for AMSR2 by NASA GSFC prior to the creation of CDR V6, so NSIDC computed them. NSIDC calculated NASA Team tie-points for the AMSR2 L1R brightness temperatures by computing a linear regression from overlapping SSMIS F17 and AMSR2 L1R brightness temperatures. We determined equivalent brightness temperatures for AMSR2 (TB_{amsr2}) corresponding to F17 (TB_{f17}) brightness temperatures, as follows:

$$TB_{f17} = m * TB_{amsr2} + b \quad (18)$$

where m and b are the slope and intercept calculated by least-squares linear regression between a year of data. Because the F17 tie-points are already known, we can then use this general relationship between brightness temperatures to compute the AMSR2 tie-points (TP_{amsr2_chan}) for each channel from the corresponding F17 tie-points (TP_{f17_chan}):

$$TP_{amsr2\_chan} = \frac{TP_{f17\_chan} - b_{chan}}{m_{chan}} \quad (19)$$

where the slope and intercept values have been computed separately for each channel. These tie-points are listed in Table 5.

3.4.2.2 Bootstrap Tie-Points

Comiso et al. (2017) designed the Bootstrap algorithm to intercalibrate between sensors similarly to the way it is done for the NASA Team algorithm where brightness temperatures from the series of sensors are regressed against each other. One sensor's brightness temperatures are adjusted to better match those from another earlier sensor. While the NASA Team tie-points are constants for each sensor, the Bootstrap algorithm uses tie-points that vary on a daily basis. The algorithm derives tie-points from analysis of clusters of brightness temperature values in the relevant channels, as in Figures 2 and 3 of Comiso (2009). The adjustment to match up sea ice fields from one sensor to the next involves a linear regression between brightness temperatures within the algorithm itself (Comiso and Nishio, 2008). Because the slope and offset values are derived each day based on the brightness temperatures, there are no specific slope/offset (tie-point) adjustments between sensors, and NSIDC did not have to perform any extra calculations to determine AMSR2 Bootstrap tie-points other than just running the algorithm.

Also, while the NASA Team originally derived the tie-points for SMMR and then adjusted future sensors to maintain consistency with SMMR, version 3.1 of the Bootstrap algorithm used AMSR-E as a baseline and adjusted SSM/I and SMMR brightness temperatures to be consistent with AMSR-E. Because AMSR-E is a newer and more advanced sensor, the intersensor calibration should be more accurate and more consistent overall. This is discussed further in Comiso and Nishio (2008) and in Comiso et al. (2017).

3.4.3 Additional Adjustments Made to AMSR2 Sea Ice Concentration Data

Despite NASA Team tie-point adjustments (section 3.4.2.1) and the adjustments done to the input AMSR2 Daily Polar Gridded Brightness Temperatures (Stewart et al., 2025) data set (section 3.3.1), the resulting sea ice concentration grids still showed a small bias in hemispheric sea ice extent between SSMIS and AMSR2 with AMSR2 generally finding more ice than SSMIS (Figure 10 and Figure 12, NH and SH, respectively). NSIDC used one final technique to account for this bias in which a varying ice/water concentration threshold is applied. We derived this method from Seki et al. (2024).

To judge the success of our technique, we looked at time series of sea ice extent from each sensor. Where there were large differences in extent, we looked at fields of concentration differences between SIC from SSMIS and SIC from AMSR2. Sometimes, the difference in extent was caused by an area of false ice due to unfiltered atmospheric effects, and sometimes there was no obvious explanation for a large difference in extent.

Aside from these few cases, we did not test for how well ice concentrations matched across entire gridded fields from SSMIS and AMSR2. We concentrated on ensuring that sea ice extent derived from concentration fields matched, since the sea ice extent parameter is used in research extensively.

Sea ice extent from passive microwave data is generally calculated using a 15% sea ice concentration threshold. Any grid cell with concentration greater than 15% is considered fully ice-covered and adds to the total extent. The threshold used will determine where the ice edge is drawn. We can adjust the SIC threshold used for AMSR2 data so that it produces an ice edge that is approximately in the same place that the 15% threshold SSMIS ice edge is.

Seki et al. (2024) pioneered this method by analyzing extent derived from AMSR-E and SSM/I during an overlap period. They applied a single concentration threshold to the entire SSM/I time series to correct the bias.

Our method differs slightly in three ways:

1. We compare ice extent data during a portion of the AMSR2 and SSMIS overlap (2023 through 2024).

2. Because there is a seasonality to the bias, we calculate a daily varying concentration threshold by performing a piecewise linear fit. The steps for this are as follows:

    a. For each hemisphere, using the years 2023 and 2024, calculate the daily extent for AMSR2 and SSMIS using a 15% concentration threshold.

    b. Smooth the extent data using a 5-day trailing average.

c. With the smoothed 2023 and 2024 data, derive a time series of differences in daily average extent from AMSR2 and SSMIS over those two years.

d. Perform a piecewise linear fit of the average difference for each hemisphere. We found that 2 breakpoints were sufficient to reasonably fit the data for either hemisphere. This gives three lines that represent the daily average extent difference with four end points at day of year 1, 111, 290, and 365 (1 January, 21 April, 17 October, and 31 December) for the Northern Hemisphere and 1, 30, 202, and 365 (1 January, 30 January, 21 July, and 31 December) for the Southern Hemisphere (see Figure 9).

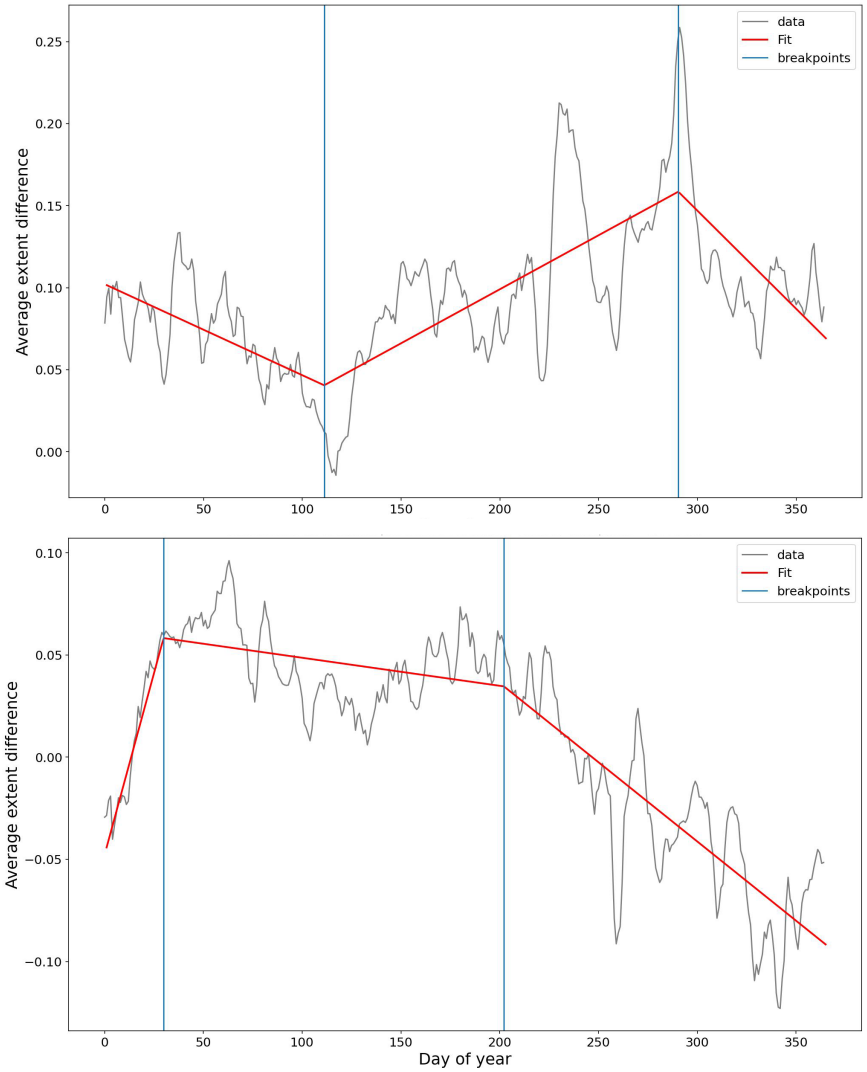

Figure 9. Piecewise linear fit of the AMSR2 average (2023-2024) for the Northern Hemisphere (top) and the Southern Hemisphere (bottom).

e. Loop through concentration thresholds from 15% to 35% for each end point day to determine at which concentration threshold the minimum difference in extent occurs. For the Northern Hemisphere, the concentration thresholds range from 24% to 28%. For the Southern Hemisphere, they range from 15% to 25%. The exact values for each day of year are provided in an ancillary file (see section 5.5.1 for details).

f. Use the concentration threshold values for the end points determined in step e along with the equations of the lines from step d, to determine a threshold for each day of the year.

3. Apply the daily varying concentration thresholds to the AMSR2 concentration grids.

The resulting AMSR2 sea ice extent record showed a reduced bias between the two sensors during the overlap period (Figure 11 and Figure 13, NH and SH, respectively).

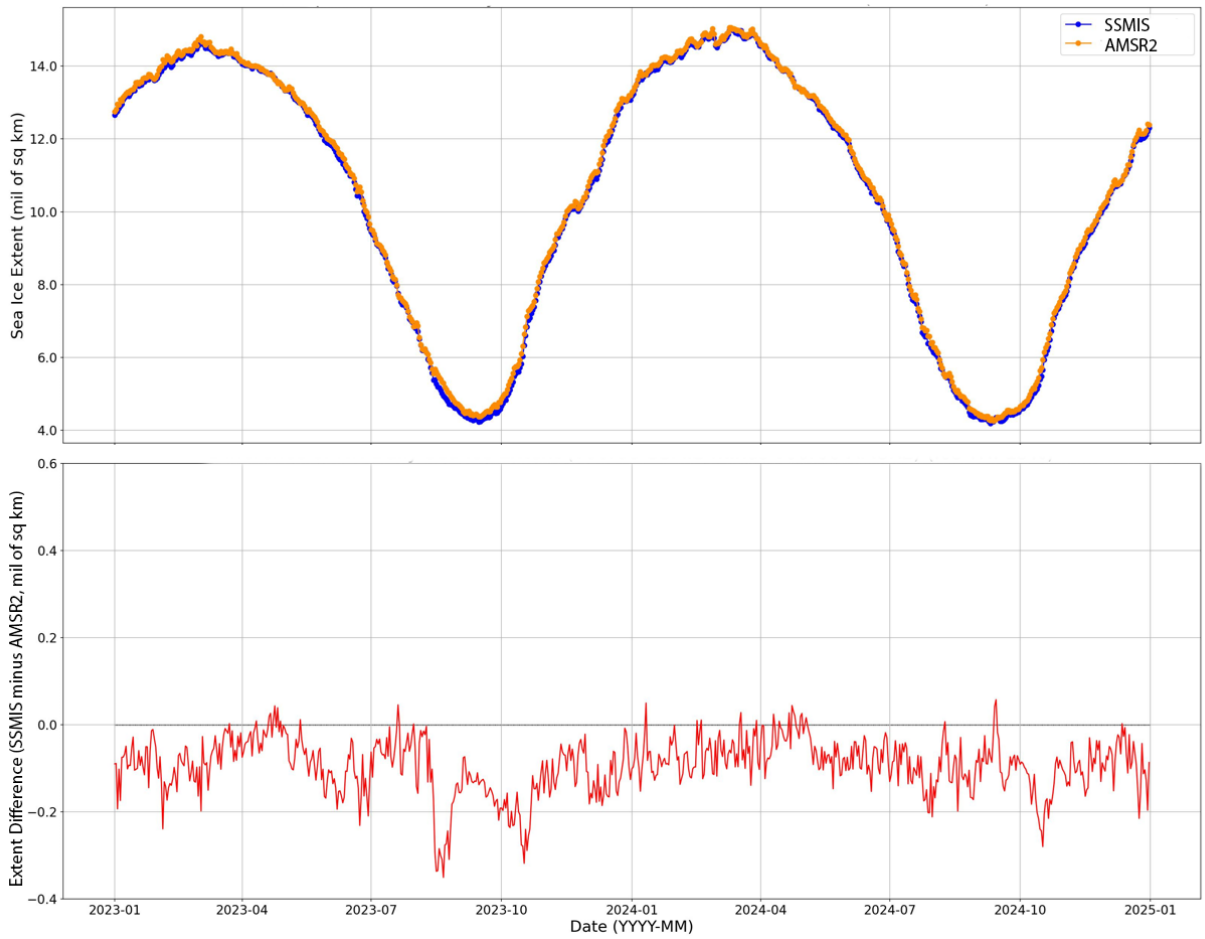

Figure 10. SSMIS- and AMSR2-derived sea ice extent for 2023 through 2024 for the Northern Hemisphere before ice concentration threshold adjustment. SSMIS extent is blue

and AMSR2 extent is orange (top). The difference between SSMIS and AMSR2 extent (bottom).

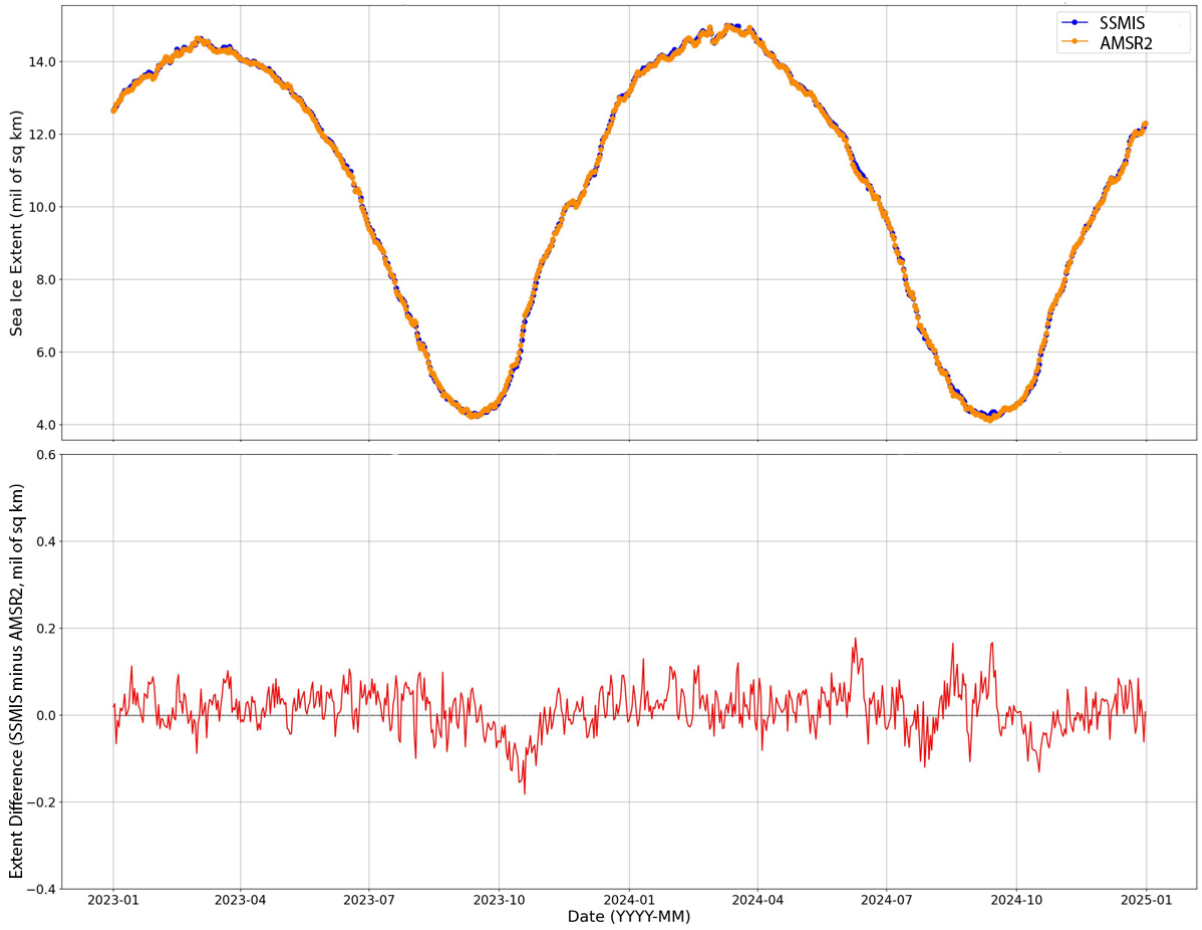

Figure 11. As in Figure 10 but with Seki ice concentration adjustment applied to AMSR2 data. SSMIS extent (blue) and AMSR2 extent (orange) for 2023 and 2024 (top), and the difference between SSMIS and AMSR2 extent (bottom).

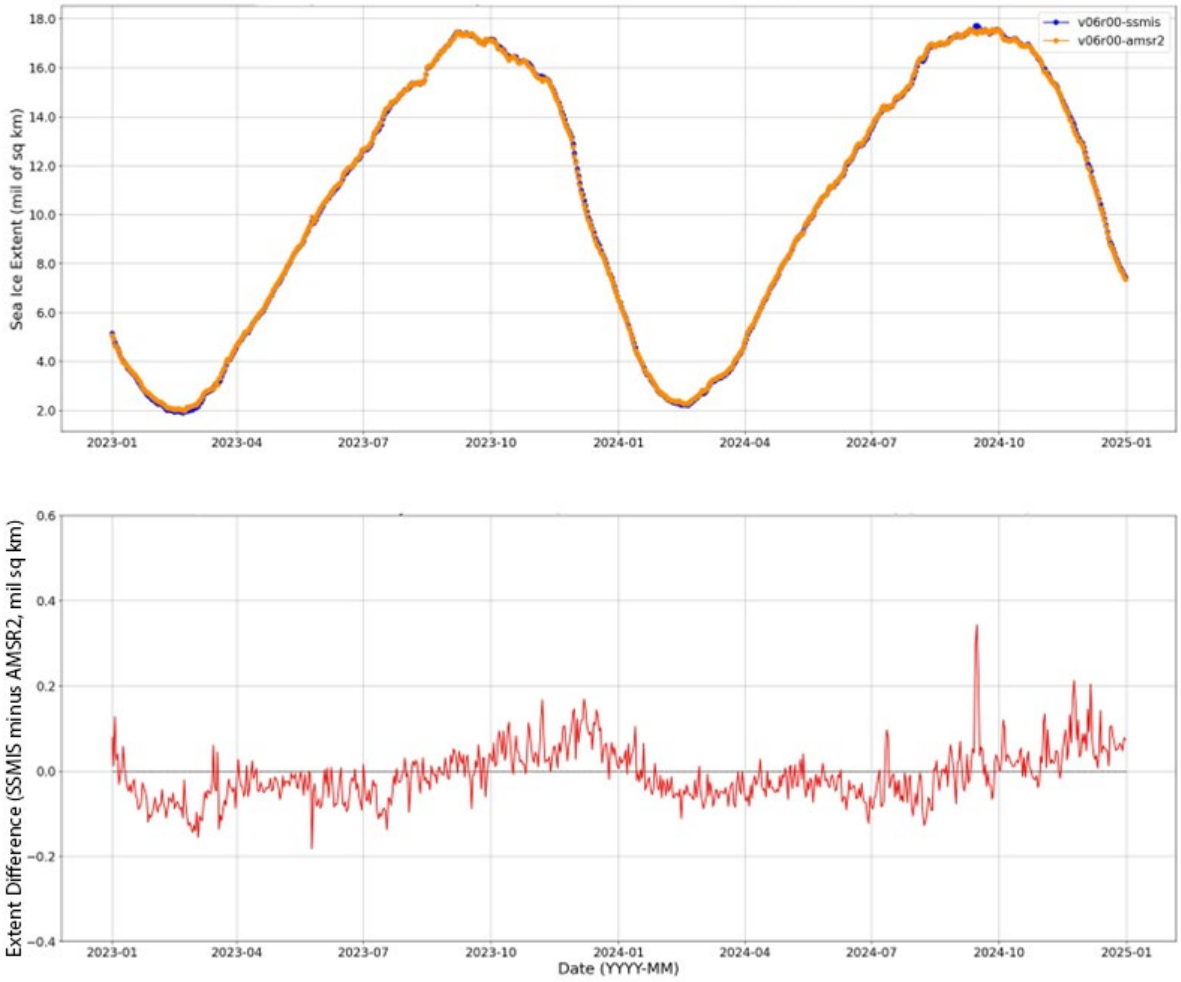

Figure 12. SSMIS- and AMSR2-derived ice extent for 2023 through 2024 for the Southern Hemisphere before ice concentration threshold adjustment. SSMIS extent is blue and AMSR2 extent is orange (top). The difference between SSMIS and AMSR2 extent (bottom).

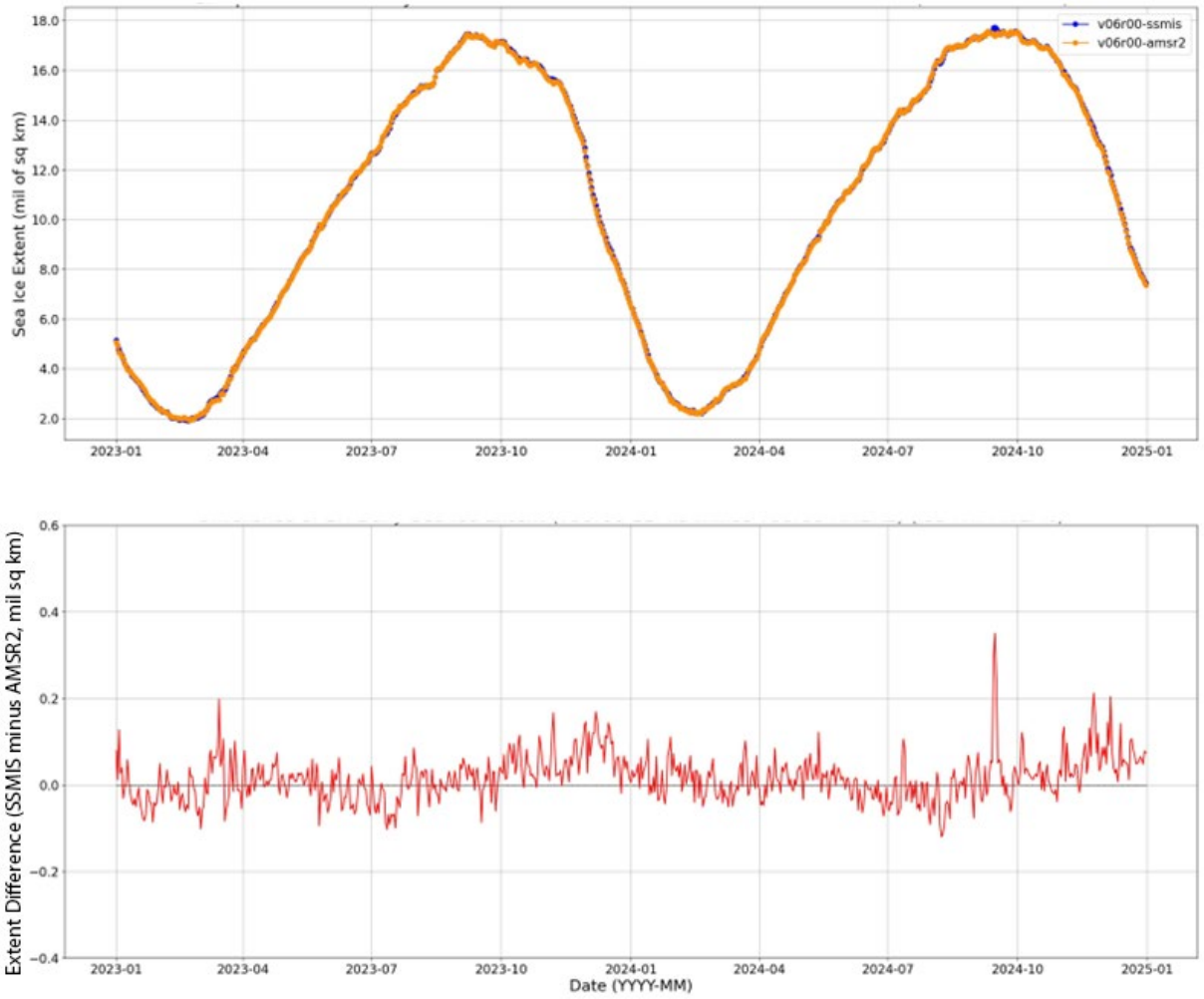

Figure 13. As in Figure 12 but with Seki ice concentration adjustment applied to AMSR2 data. SSMIS extent (blue) and AMSR2 extent (orange) for 2023 and 2024 (top), and the difference between SSMIS and AMSR2 extent (bottom).

3.4.4 Algorithm Output

The sea ice CDR code creates daily and monthly netCDF (network Common Data Form) data files for each hemisphere. Each daily and monthly CDR file contains four primary CDR fields: a CDR concentration estimate, a standard deviation field, a melt onset flag, and a quality assessment field. Each field is on the 25 km polar stereographic grid: 304 columns by 448 rows for the Northern Hemisphere (EPSG 3411) and 316 columns by 332 rows for the Southern Hemisphere (EPSG 3412). In the two sub-sections below, the daily and the monthly fields are described in detail.

Note: In addition to the individual daily and monthly netCDF files, aggregated versions of these files are also produced. For the daily files, there are yearly aggregated files, where a year's worth of daily data is stored in one netCDF file. For the monthly files,

there is one period-of-record file for each hemisphere where all the monthly data are stored in one netCDF file per hemisphere.

3.4.4.1 Fields in the daily CDR files

The daily files contain the following variables and groups:

1. cdr_seaice_conc
2. cdr_seaice_conc_interp_spatial_flag
3. cdr_seaice_conc_interp_temporal_flag
4. cdr_seaice_conc_qa_flag
5. cdr_seaice_conc_stdev
6. cdr_supplementary (group)
    a. cdr_melt_onset_day
    b. latitude (aggregated files only)
    c. longitude (aggregated files only)
    d. raw_bt_seaice_conc
    e. raw_nt_seaice_conc
    f. surface_type_mask
7. crs
8. time
9. x
10. y

These CDR fields are explained below.

1. Sea Ice Concentration CDR

   This field, named cdr_seaice_conc, contains the sea ice concentration values for the CDR, scaled from 0-100%. See Section 3.4.1.3 for details on how this is calculated.

2. Spatial Interpolation QC Flag

   This field, named cdr_seaice_conc_interp_spatial_flag, is set for spatially interpolated grid cells. The values are described in Table 7.

Condition	Flag Value	Label in NetCDF Variable
19 GHz vertical brightness temperature spatially interpolated	1	19v_tb_value_interpolated
19 GHz horizontal brightness temperature spatially interpolated	2	19h_tb_value_interpolated
22 GHz vertical brightness	4	22v_tb_value_interpolated

temperature spatially interpolated		
37 GHz vertical brightness temperature spatially interpolated	8	37v_tb_value_interpolated
37 GHz horizontal brightness temperature spatially interpolated	16	37h_tb_value_interpolated
Pole hole spatially interpolated (Arctic only)	32	pole_hole_spatially_interpolated

Table 7. Spatial interpolation flag values. A grid cell that satisfies more than one criteria will contain the sum of all applicable flag values.

3. Temporal Interpolation QC Flag

   This field, named cdr_seaice_conc_interp_temporal_flag, provides details on the grid cells that were temporally interpolated. This flag uses one- or two-digit numbers to indicate the known data points used in the interpolation. For two-sided gap filling, it is always a 2-digit number where the first digit indicates the number of days in the past, while the second digit indicates the number of days in the future from which the data point came from, with a max of five days in either direction. For example, a flag value of 24 indicates that the missing grid cell was linearly interpolated using sea ice concentration data from two days prior and four days in the future. In the two-sided method, the flag values range from 11 to 55 but exclude 10, 20, and 30. For the one-sided gap filing, where only one day is used, the value can be one or two digits with possible values of 1, 2, 3, 10, 20, and 30. Two-digit values indicate that data in the past were used, while single digit values indicate that data in the future were used. For example, a value of 30 indicates that data from three days in the past was copied. See section 3.4.1.4.1 for more information on the temporal interpolation method.

   Note: For the near-real-time ICDR, the temporal interpolation is only backward-looking and the algorithm allows for looking back up to five days.

4. Quality Assessment (QA) Flags

   This field, named cdr_seaice_conc_qa_flag, provides additional assessment to complement the standard deviation field. This field includes flags for the following conditions: if the BT and NT weather filters were applied, if land-spillover corrections were applied, if the invalid ice mask was applied, if spatial or temporal interpolation was applied, and the melt state (Table 8).

   Note: The melt-state flag can be used in conjunction with the cdr_melt_onset_day variable. The melt-state flag simply identifies that melt has been detected but the melt onset variable provides the day of year of melt onset.

The melt-state flag is used starting on day of year 60, around the time when the maximum sea ice extent is reached each year. Once a grid cell is flagged as melting, it remains so through the rest of the summer (day of year 244), roughly the time when extent reaches its minimum value. When the sea ice concentration is zero, the flag will be turned off. In other words, the flag will only be on if melt conditions are met and there is sea ice. Note this is different from the cdr_melt_onset_day variable which, once set, shows the day of melt onset through the rest of the year. Table 8 lists the flag values in the QA field, with an explanation for each parameter. Grid cells with more than one flag property contain the sum of both flags. In general, higher values are more likely to have high errors. Note that 0 is the fill value for this variable.

Condition	**Flag Value**	**Label in NetCDF Variable**
BT weather filter applied	1	BT_weather_filter_applied
NT weather filter applied	2	NT_weather_filter_applied
Land-spillover correction applied (either NT2 or BT)	4	Land_spillover_filter_applied
No T_B input data available	8	No_input_data
Invalid ice mask applied	16	invalid_ice_mask_applied
Spatially interpolation applied	32	spatial_interpolation_applied
Temporal interpolation applied	64	temporal_interpolation_applied
Start of Melt Detected (Arctic only)	128	melt_start_detected

Table 8: List of flag values used in the daily CDR QA field. A grid cell that satisfies more than one criteria will contain the sum of all applicable flag values.

5. Standard Deviation of Sea Ice Concentration

This field, named cdr_seaice_conc_stdev, contains the standard deviation of both the NASA Team and Bootstrap concentration estimate at each ocean/sea ice grid cell for that grid cell and the surrounding 8 grid cells (Figure 14). The standard deviation is calculated from the total of two 3 x 3 arrays of grid cells (one of NASA Team concentrations and one of Bootstrap concentrations), for 18 grid cells in total. Land grid cells within the 3 x 3 array are not included in the calculation; thus, along the coast, fewer than 18 values are used. Any missing grid cells (for example, the pole hole in the Northern Hemisphere) are also not included in the standard deviation. A minimum of 6 valid concentration values out of the 18 total are required to compute a standard deviation. Thus, some grid cells within small bays and inlets may not have a standard deviation value; such cells are likely to be potentially affected by land-spillover and should be considered to have high uncertainties.

This field is meant to give an indication of the uncertainties in the daily CDR concentration estimate. It is not a quantitative error estimate and should not be used as such. However, it does provide a useful guide to users as to the relative accuracy of concentration estimates relative to surrounding grid cells and can be used to derive relative weights for comparisons, interpolations, or assimilation studies. In winter conditions, away from the ice edge or coast where spatial variability occurs, standard deviations are typically a few percent (Cavalieri et al., 1984) and can potentially serve as a quantitative upper limit of the concentration error (Gloersen et al., 1993).

The error sources for sea ice concentration are described in detail below, but high standard-deviation values will generally correspond to regions where concentration errors are likely higher.

First, isolated sea ice grid cells along the coastline that result from the land-spillover issue discussed previously will have higher standard deviations compared to ice-free ocean or high concentration ice cover along the coast because of the mixture of ice and open water (0% ice) in the calculation.

Another region of higher errors occurs along the ice-water boundary (the ice edge) due to limitations in the sensor resolution, to motion of the ice during the 24-hour average period, and to melt/growth of ice. These high gradient regions will have high standard deviation values.

Finally, during melt, the surface and atmospheric effects become relatively larger, leading to more spatial variability and higher standard deviation values. The melt also tends to cause the algorithms to underestimate concentration because they incorrectly interpret the surface melt on top of the ice as increased open water. The NASA Team concentrations generally have a large low bias compared to the Bootstrap concentrations. This is the rationale for computing the standard deviation from both algorithms instead of the combined CDR estimate or just one of the algorithms. The lower relative bias in the NASA Team during melt compared to Bootstrap will yield increased standard deviation values, better indicating the presence of melt than using only the CDR concentration standard deviation. Standard deviation values range from 0-1, and the fill value is -1.

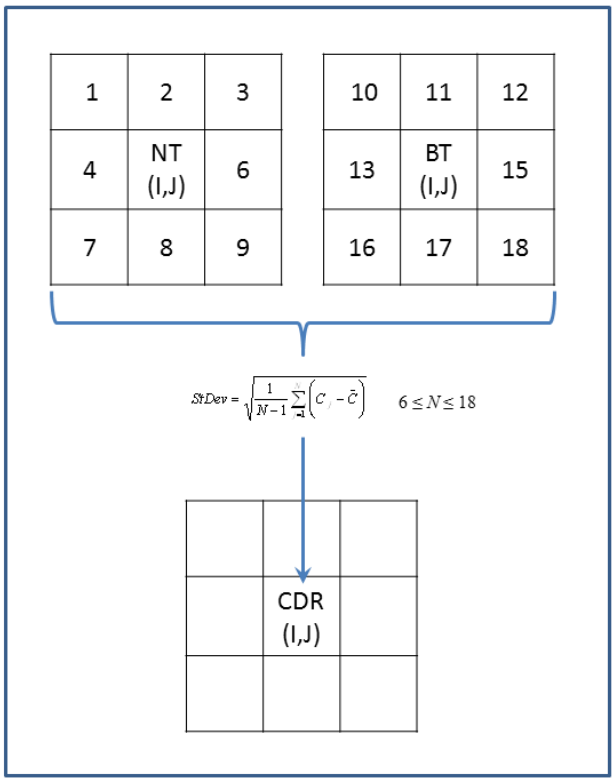

Figure 14: Schematic of grid cell values used in calculation of the CDR standard deviation field. All non-missing ocean/sea ice concentration values (C), from both the NASA Team and Bootstrap algorithm, of the 3 x 3 box surrounding each (I,J) grid cell (up to 18 total values) are used to calculate the standard deviation. A minimum of six grid cells with valid values is used as a threshold for a valid standard deviation.

6. Supplementary Data Group

   All supplementary variables are held within the cdr_supplementary group for organizational purposes. The variables included in this group are cdr_melt_onset_day, latitude, longitude, raw_bt_seaice_conc, raw_nt_seaice_conc, and surface_type_mask. They are described below.

   a. Day of Melt Onset

      This field, named cdr_melt_onset_day, contains the day of year on which melting sea ice was first detected in each grid cell. The melt onset day is only calculated for the melt season: days 60 (March 1/Feb 29 for leap years) through 244 (September 1/August 31 for leap years), inclusive. Once detected, the value is retained for the rest of the year. For example, if a grid cell started melting on day 73, the value for the grid cell on that day will be 73, as will all subsequent days until the end of the year when it is then reset to the fill value of 255. Before melting is detected or if no melt is ever detected for that grid cell, the value will be 255.

One of the largest contributors to errors in concentration estimates occurs when surface melt begins (see Section 4.2.5). Thus, a melt-quality flag is implemented in the Northern Hemisphere to indicate where melt may be occurring. The melt onset test is performed only in the Northern Hemisphere because the character of the ice cover in the Southern Hemisphere, typified by strong melt-refreeze cycles, does not yield a reliable melt threshold in passive microwave brightness temperature data (Willmes et al., 2009).

The melt flag is a near-real-time version of the Drobot and Anderson (2001) algorithm, which uses a brightness temperature difference threshold to determine whether melt has begun for the overlying snow cover at each sea ice grid cell. The algorithm is implemented as follows:

$$T_B(19H) - T_B(37H) > 2K \rightarrow no\ melt \quad (20)$$

$$T_B(19H) - T_B(37H) \leq 2K \rightarrow melt\ has\ begun \quad (21)$$

A long-term melt onset climate dataset, *Snow Melt Onset Over Arctic Sea Ice from SMMR and SSM/I-SSMIS Brightness Temperatures* (Bliss et al., 2022), is distributed by NSIDC. That dataset includes a 20-day temporal filter to screen out possible false melt signatures. For simplicity, the temporal filter is not employed in this product. This means that some grid cells flagged as melt may not actually be melting, and thus, the flag is more conservative than the climate dataset. Note that the melt test does not consider any effects of sea ice motion. Also note that melt may be intermittent initially in the spring (melt, then refreeze, and melt again) and freeze-up begins near the pole well before September 1. Thus, grid cells that are flagged as melt may not actually have melt occurring and the flag should be used only as a guide for the data quality of the CDR concentration estimates and should not be used specifically for studies on melt.

The conditions for melt onset at a particular grid cell are the following:

- Melt detected:
    - Concentration ≥ 50% at the beginning of the season
    - Grid cell is not land, coast, shore (1 grid cell from coast), near-shore (2 grid cells from coast), or lake
- Current sea ice concentration ≥ 50%
- Brightness temperature delta (19H - 37H) < 2K (Drobot and Anderson, 2001)
- Presence of brightness temperatures for both channels (19H, 37H)

Note: To calculate the melt onset for SSMIS data, the input brightness temperatures are first scaled as follows:

$$19H\_scaled = 1.021 * 19H - 1.681 \quad (22)$$

$$37H\_scaled = 1.001 * 37H - 0.650 \quad (23)$$

These equations were derived by a regression between SSMIS F17 and SSMIS F13 brightness temperatures during March through September 2007 when there was an overlap period between the two satellites. Regressions were run for each daily average brightness temperature field and slope and intercept values were calculated. These daily slope and intercept values were then averaged over the entire March through September period to derive the equations above.

The reason for applying this adjustment is to help minimize differences between the F17 and F13 sensors, including sensor characteristics (sensor footprint, geometry), differences in orbit (time of equatorial crossing), etc. For the melt onset, Equations 22 and 23 are used to make this adjustment.

b. Latitude

Latitude in degrees north. Note this is found in the aggregated daily netCDF files only and not in the individual daily netCDF files.

c. Longitude

Longitude in degrees east. Note this is found in the aggregated netCDF files only and not in the individual daily netCDF files.

d. NSIDC Raw Bootstrap Sea Ice Concentrations

NSIDC includes the intermediate NSIDC processed raw daily Bootstrap sea ice concentration, named raw_bt_seaice_conc, in the product suite to provide transparency in the creation of the sea ice CDR product.

These data are similar to the GSFC produced NASA team sea ice concentrations available from NSIDC as the *Bootstrap Sea Ice Concentrations from Nimbus-7 SMMR and DMSP SSM/I-SSMIS* (Comiso, 2023) except that the weather filters and land-spillover corrections have not been applied.

e. NSIDC Raw NASA Team Sea Ice Concentrations

NSIDC includes the intermediate NSIDC processed raw daily NASA Team sea ice concentration, named raw_nt_seaice_conc, in the product suite to

provide transparency in the creation of the sea ice CDR product.

These data are similar to the GSFC produced NASA team sea ice concentrations available from NSIDC as the *Sea Ice Concentrations from Nimbus-7 SMMR and DMSP SSM/I-SSMIS Passive Microwave Data* (DiGirolamo et al., 2022) except that the weather filters and land-spillover corrections have not been applied.

f. Surface type mask

This field, named surface_type_mask, provides a mask of different Earth surface types.

The values are the following:
50: ocean
75: lake
100: polehole_mask (Arctic only)
200: coast (land adjacent to ocean)
250: land

7. Coordinate Reference System

This field, named crs, describes the polar stereographic projection information for these data.

8. Time

The date of the data (days since 1970-01-01).

9. Xgrid

The projection grid x centers in meters.

10. Ygrid

The projection grid y centers in meters.

3.4.4.2 Fields in the monthly CDR files

The monthly fields are created from all daily files in the given month. The monthly files contain the following variables and groups:

1. cdr_seaice_conc_monthly
2. cdr_seaice_conc_monthly_qa_flag
3. cdr_seaice_conc_monthly_stdev
4. cdr_supplementary (group)
   a. cdr_melt_onset_day_monthly
   b. latitude (aggregated file only)
   c. longitude (aggregated file only)
   d. surface_type_mask
5. crs
6. time
7. x
8. y

These CDR fields are explained below:

1. Sea Ice Concentration CDR

   This field, named cdr_seaice_conc_monthly, contains the monthly average sea ice concentration values for the CDR, scaled from 0-100%. See Section 3.4.1.3 for details on how this is calculated.

2. Quality Assessment (QA) Flags

   This field, named cdr_seaice_conc_monthly_qa_flag, contains flags that provide additional information about the monthly averages. The flags are listed in Table 9. They include a flag for when the average concentration of a grid cell exceeds 15%. A 15% concentration contour is commonly used to define the ice edge, so summing cells that hold this flag can be used to easily map and quantify the total extent. Another flag indicates when average concentration exceeds 30%, which is a commonly used alternate ice edge definition. Users may want to remove lower concentration ice that tends to have higher errors. Another flag indicates whether at least half the days have a concentration greater than 15%. This provides a monthly median extent, which may be a better representation of the monthly ice presence because an average conflates the spatial and temporal variation through the month. Additionally, there is a flag that indicates whether at least half the days have a concentration greater than 30%. This also provides a monthly median extent, but this higher percentage may leave out questionable or erroneous ice. There are flags to show if a cell was masked by the invalid ice mask and whether spatial or temporal interpolation was performed. Finally, there is a flag to note whether melt was detected during the month. Since melt tends to

bias concentrations lower, this flag gives a sense of whether melt is having a dominating effect.

Condition	Flag Value	Label in NetCDF File
Average concentration exceeds 15%	1	average_concentration_exceeds_0.15
Average concentration exceeds 30%	2	average_concentration_exceeds_0.30
At least half the days have sea ice conc > 15%	4	at_least_half_the_days_have_sea_ice_conc_exceeds_0.15
At least half the days have sea ice conc > 30%	8	at_least_half_the_days_have_sea_ice_conc_exceeds_0.30
Invalid ice mask applied	16	invalid_ice_mask_applied
At least one day during month has spatial interpolation	32	at_least_one_day_during_month_has_spatial_interpolation
At least one day during month has temporal interpolation	64	at_least_one_day_during_month_has_temporal_interpolation
Melt detected (at least one day of melt occurred during the month >= 1)	128	at_least_one_day_during_month_has_melt_detected

Table 9: List of flag values used in the monthly CDR QA bit mask. A grid cell that satisfies more than one criterion will contain the sum of all applicable flag values. For example, if spatial interpolation was performed and melt detected then the value will be 160 (32 + 128).

3. Standard Deviation of Concentration

This field, named cdr_seaice_conc_monthly_stdev, contains the standard deviation (with one degree of freedom) of the daily concentrations in the month. As in the monthly concentration, a minimum of 20 days is required for a valid monthly value. Note that while the daily concentration standard deviation field is based on the variability of the NT and BT concentrations over a 3 x 3 grid cell spatial region, this monthly field is simply the standard deviation of the daily CDR concentrations – i.e., a temporal standard deviation for each grid cell.

4. Supplementary Data Group
   All supplementary variables are held within the cdr_supplementary group for organizational purposes. The variables included in this group are cdr_melt_onset_day_monthly, latitude (aggregated file only), longitude (aggregated file only), and surface_type_mask. They are described below.

   a. Day of Melt Onset

      This field, named cdr_melt_onset_day_monthly, contains the day of year on which melting sea ice was first detected in each grid cell. For the monthly data, this is the value from the last day of the month. The melt onset day is only calculated for the melt season: days 60 (March 1/February 29 for leap years) through 244 (September 1/August 31 for leap years), inclusive. Once detected, the value is retained for the rest of the year. For example, if a grid cell started melting on day 73, the variable for the grid cell on that day will be 73, as will all subsequent days until the end of the year. Before melting is detected or if no melt is ever detected for that grid cell, the value will be 255.

   b. Latitude

      Latitude in degrees north. Note this is found in the aggregated monthly netCDF files only and not in the individual monthly netCDF files.

   c. Longitude

      Longitude in degrees east. Note this is found in the aggregated netCDF files only and not in the individual monthly netCDF files.

   d. Surface Type Mask

      This field, named surface_type_mask, provides a mask of different Earth surface types.

      The values are the following:
      50: ocean
      75: lake
      100: polehole_mask (Arctic only)
      200: coast (land adjacent to ocean)
      250: land

5. CRS

   Describes the polar stereographic projection information for these data.

6. Time

   The date of the data (days since 1970-01-01).

7. X

   The projection grid x centers in meters.

8. Y

   The projection grid y centers in meters.

4. Test Datasets and Outputs

4.1 Test Input Datasets

We tested the CDR Version 6 code by comparing its concentration fields with existing products and checking for any large differences that might indicate errors in our implementation of the NASA Team or Bootstrap algorithm. Existing products include CDR Version 5, and originally, *Sea Ice Concentrations from Nimbus-7 SMMR and DMSP SSM/I Passive Microwave Data* (DiGirolamo et al., 2022) and *Bootstrap Sea Ice Concentrations from Nimbus-7 SMMR and DMSP SSM/I* (Comiso, 2022).

4.2 Test Output Analysis

4.2.1 Reproducibility

Peng et al. (2013) and Meier et al. (2014) indicated that the Version 3 CDR algorithm reasonably reproduces the original NASA Team and Bootstrap concentration fields from SSMI and SSMIS provided by NASA GSFC except for the manual corrections and gap-filling interpolations applied by GSFC. For version 4, NSIDC confirmed that the consistency with GSFC extends into the SMMR sensor period, and the added spatial and temporal interpolation that addresses data gaps achieves consistent results with the GSFC products. For version 6, we tested against the Version 5 CDR to confirm reproducibility.

Note, NSIDC obtained the original C and Fortran program code for the NASA Team algorithm from N. DiGirolamo (personal communication, May 2020) and for the Bootstrap algorithm from R. Gersten (personal communication, April 2022), both at NASA GSFC. NSIDC developers then refactored that code into Python. Within the confines of producing a CDR, we have attempted to implement the algorithms and incorporate similar automatic filtering and quality control features to be as consistent as possible with the heritage data products from NASA GSFC while at the same time implementing improvements that produced the most consistent results for the CDR product.

4.2.2 Precision and Accuracy

The precision and accuracy of the NASA Team and Bootstrap algorithms, when used with the SSM/I and SSMIS data, have been evaluated in numerous studies over the years as noted in the following sections. These assessments have not been rigorous evaluations done with a validation data set. Therefore, it may be better to say they estimate uncertainty rather than accuracy, but because most use the term “accuracy” we retain it here.

Assessments have been comparisons that have typically used coincident airborne or satellite remote sensing data from optical, thermal, or radar sensors, generally at a

higher spatial resolution than the SSM/I and SSMIS instruments but with only local or regional coverage. Several assessments, including ones that use the AMSR sensors, indicate a precision of ~5% with an accuracy of ~10% during mid-winter conditions away from the coast and the ice edge (Steffen et al., 1992; Gloersen et al., 1993; Comiso et al., 1997; Meier et al., 2005; Andersen et al., 2007; Belchansky and Douglas, 2002; Meier et al., 2017; Kern et al., 2019). However, uncertainties are higher under some conditions – most notably near the ice edge and when the surface is undergoing melt. Kwok (2002) found that passive microwave overestimates open water by three to five times in winter. Partington et al. (2003) performed a study with the SSM/I instruments and found a difference with operational charts that was relatively low in the winter but rose to more than 20% in summer. In addition, while filters remove many artifacts, some erroneous ice can still occur over the open ocean due to weather effects and along the coast due to land-spillover effects (i.e., mixed ocean and land grid cells).

The precision and accuracy, or uncertainty, of the NASA Team and Bootstrap algorithms when used with the JAXA L1R AMSR2 data has not been assessed. Kern et al. (2020) included the 12.5 km resolution AMSR2 in an intercomparison of passive microwave SIC data during arctic summer with the MODerate resolution Imaging Spectroradiometer (MODIS). Kern et al. compared SIC data with a MODIS-derived melt pond fraction and found that all passive microwave products underestimate SIC by a large amount in the summer but the data group utilizing 12.5 km AMSR2 data was the closest match to MODIS. Since the SIC CDR uses a resampled 25 km AMSR2 product, it is likely that the AMSR2 data in the CDR is not as close a match to MODIS as in the Kern et al. (2020) study and is probably more like SSMIS.

Figure 15 shows a representative comparison of sea ice from the SIC CDR V6 using SSMIS and AMSR2, along with a visible composite MODIS image during the summer of 2021. Even after being resampled to the SSMIS resolution, the 25 km gridded AMSR2 concentration field seems to depict the ice cover slightly better than SSMIS, especially near the bottom of the images along the coast of Greenland where SSMIS shows ice but AMSR2 and MODIS do not. However, this is only one point in time of these data, so it is not conclusive.

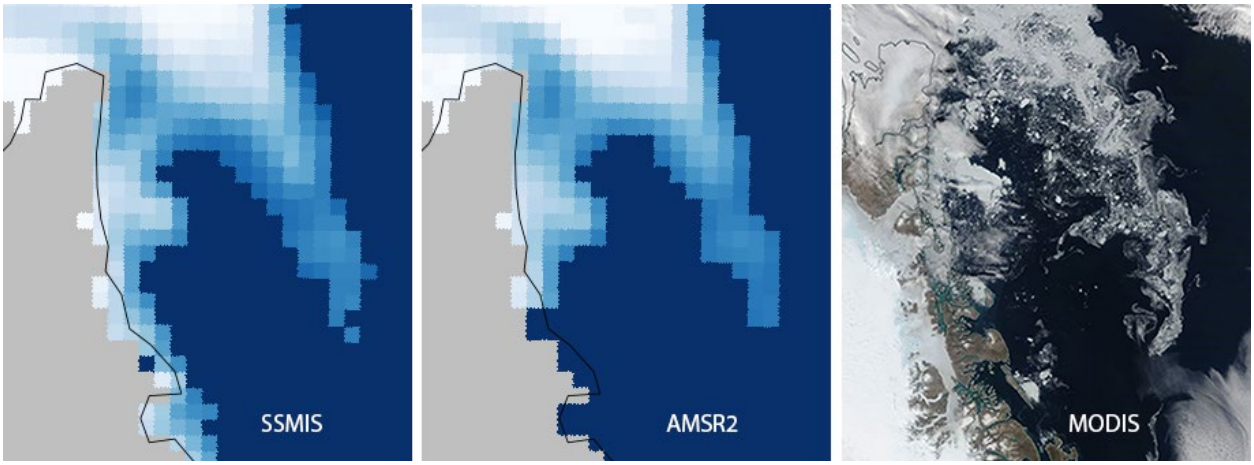

Figure 15. Comparison of SIC from 25 km SSMIS CDR (left), 25 km AMSR2 CDR (middle), and 500 m MODIS for 30 July 2021 off the northeast coast of Greenland.

Fetterer et al. (2023) compared a year of sea ice concentration from a NOAA Visible Infrared Imaging Radiometer Suite (VIIRS) data set (Liu and Key, 2019, available from NOAA CoastWatch) with sea ice concentration from an earlier, 12.5 km, AMSR2 SIC prototype. VIIRS visible and near-IR band data offer high resolution, but clouds severely limit the usefulness of the derived sea ice product for a validation study, and results were inconclusive.

While the errors enumerated in the remainder of Section 4.2 were derived in studies that used DMSP data, they apply to higher-resolution AMSR2 data as well. For example, ice concentration is likely to be underestimated by AMSR2 as well as by SSMIS in areas with a lot of thin ice. However, because the higher resolution of AMSR2 delineates areas of different ice types more precisely, the underestimation is likely to be confined to a smaller area. See the discussion of spatial smearing in Section 4.2.4.

4.2.3 Error Budget

Errors can come from many sources including problems with the sensor, surface variation, weather effects, and inadequacies in the algorithm. Atmospheric water vapor is a weather effect that can modulate the passive microwave signature of the surface, particularly at the 19 GHz frequency, causing ice concentration to be overestimated. While the emissivity of seawater is quite constant, that of sea ice varies considerably depending on many factors including age, thickness, surface roughness, and melt state. This and other concentration error sources have been examined to some extent in Andersen et al. (2007), and their influence appears to be small compared to the estimated sea ice trends, but such effects should be kept in mind when using these data.

When one considers that algorithms must arrive at a single number for ice concentration considering the varying brightness temperatures of all the different surface types that may fill the footprints of the 19 GHz and 37 GHz channels and that those footprints

differ in size and shape across the instrument swath, one can appreciate the difficulty of the problem. *Microwave Remote Sensing of Sea Ice* includes chapters that provide a comprehensive overview of the subject (Carsey, 1992).

Table 10 summarizes the error sources, expected potential magnitude of the error, the spatial and/or temporal regime, and the relative effect on each algorithm (BT, NT). These are ranges of typical values as reported in the cited validation studies. Errors at any given grid cell may be larger. These error sources are described in sections 4.2.4, 4.2.5, and 4.2.6. Note that many errors will be mitigated in the monthly average fields. Consequently, monthly averages are generally of better science quality – more stable and better suited for climate analyses.

Error Source	Typical Magnitude and Bias (if any)	Spatial/Temporal Regime	Relative Effect on Algorithm
Sensor Noise	+/-1%	All	NT and BT similarly
Calibration Drift	Undetermined/ minimal	All	NT and BT similarly
IFOV/Gridding	<5%	Winter, pack ice	NT and BT similarly
IFOV/ Gridding	0-100%	Sharp gradients (e.g., ice edge, coast)	NT and BT similarly
Intersensor calibration	~0.1%	All	NT and BT similarly
Physical temperature	<5%, low	Winter, cold	BT more than NT
Non-melt surface variation	<5%, low	Winter, central pack ice	NT more than BT
Thin ice	~30-50%, low	Near ice edge, fall freeze-up	NT more than BT
Surface melt	~10-30%, low	Summer	NT more than BT
Wind	5-20%, high	Open water	NT and BT similarly
Water Vapor, Liquid Water	0-20%, high	Open water and ice near edge	NT and BT similarly

Table 10: List of error sources and typical error magnitudes in % concentration for the NASA Team (NT) and Bootstrap (BT) algorithms with biases and typical regimes. A low bias means that the error source contributes to underestimating the true concentration by the indicated range; high bias is the opposite.

4.2.4 Errors from Sensor Characteristics

There are four errors that come from the sensor characteristics: (A) sensor noise, (B) the transition between sensors, (C) the large IFOV of the sensors, and (D) the 24-hour composite.

A. One source of error is simply from sensor noise. The SSM/I and SSMIS sensors have been found to have an RMS error of 0.5 K to 1.0 K (Wentz, 1997). A sensitivity study of NASA Team algorithm concentration found that the concentration sensitivity is about 1-2% per 1 K (Gloersen et al., 1993). The algorithm precision is about 1% (Imaoka et al., 2010; Ishikawa et al., 2017). In addition, a satellite's orbit may drift over time, which may degrade an instrument's data quality and increase the sensor noise. Most SSM/I and SSMIS instruments were in use long past their designed lifetime expectancy.

B. Potential sensor errors may result from the transition between sensors on different satellites. The brightness temperature regression and tie-point adjustment correct for this, though small artifacts remain (Cavalieri et al., 1999; Comiso and Nishio, 2008). Comparison of ice extent estimates from sensor overlap periods indicate that the brightness temperature adjustments yield agreements that are on the order of 0.05% or less and about 0.5% for sea ice area (Cavalieri et al., 1999; Cavalieri et al., 2011). Short overlap periods of early sensor transitions (SMMR to SSM/I F8 and SSM/I F8 to SSM/I F11) may not account for the full seasonal variability (Meier and Khalsa, 2011; Cavalieri et al., 2011) and differences may be higher in some cases. However, differences appear to be well below the sensitivity of the instrument, thus providing confidence in the robustness of the intercalibrated algorithms through the time series.

C. A more significant limitation of the sensors is the large sensor footprint (IFOV) of the instruments. Though all input brightness temperatures are gridded to the 25 km polar stereographic grid, the IFOV of the sensors is coarser than this (Table 2); they can be as large as 72 km x 44 km for the 19 GHz channel. This means that the sensor is obtaining information from up to a 3 x 2 region of 25 km grid cells (~ 75 km x 50 km), but that signature is placed into a single 25 km grid cell. This results in a spatial "smearing" across several grid cells, so any spatial variability on a smaller scale may be missed. Further, because a simple drop-in-the-bucket gridding method is used, some grid cells do not coincide with the center of a sensor footprint so do not have a brightness temperature directly assigned to them even though they are partially covered by at least one footprint. The course resolution also leads to the land-spillover issue of grid cells with a mixture of land and water brightness temperatures that can be interpreted by the algorithms as sea ice along the coast.

D. Another issue is the use of 24-hour composite average brightness temperatures as input for the concentration algorithms. Sea ice can drift with the winds and ocean currents over a 24-hour period, and the surface properties of the sea ice can also change considerably. This means that the daily brightness temperature fields of the surface properties at a given grid cell are an amalgamation of conditions over 24 hours.

   Some of the effects caused by this spatial and temporal compositing of the

brightness temperatures is ameliorated because these data have been used consistently for algorithm development, tie-point derivation, and intersensor adjustment. Thus, these effects, while limiting accuracy on a grid cell level, still yield consistent large-scale trends and variability in the sea ice cover. Regions with sharp gradients in brightness temperature, such as the ice edge and the land/water boundary, are most affected by these characteristics.

Of note is the compositing effect on the precision of the ice edge. First, the ice edge is a region of sharp brightness temperature gradients and rapid (less than 24 hour) variability. Second, there is necessarily ambiguity in the ice edge location due to the limited spatial resolution. For example, an ice edge grid cell with a 50% concentration could mean that the entire cell has a uniformly distributed 50% ice concentration, that half of the grid is covered by 100% ice and the other half is ice free, or something in between. Because the true spatial resolution is limited by the sensor IFOV and not the grid cell area, even with perfect data and a perfect algorithm, the ice edge can in principle only be discerned to within ~50 km. However, the distance between the passive microwave observed (15% concentration) edge and the true ice edge, as determined in ship observations (Ozsoy-Cicek et al., 2009; Ozsoy-Cicek et al., 2011), operational sea ice charts (Partington, 2000), or high-resolution satellite data (Meier et al., 2003; Meier, 2005), may be much larger than that.

4.2.5 Errors Due to Surface Variation

There are four primary error sources from surface variation: (A) ice type, (B) ice surface variation, (C) physical temperature, and (D) surface melt.

A. While five passive microwave channels are potentially available for discriminating sea ice types, not all are completely independent and in practice only three surface types are retrievable, one water and two ice (multiyear and first-year). However, two ice types cannot fully describe the complex surface of the sea ice. Tie-points are derived based on “pure surface types” of 100% ice, typically for thick multiyear or first-year ice (for the Arctic). The actual emission from thin ice (as indicated by the brightness temperature) varies with ice thickness up to perhaps 30 cm. Thin ice cover appears in the algorithms as a mixture of water and thick ice; so, thin ice concentration is often underestimated. Algorithms using specific thin ice tie-points have been developed (Cavalieri, 1994), but these are not applicable for hemispheric datasets. Because ice quickly grows thicker in winter months, thin ice tends to constitute a small fraction of the overall ice cover but can result in large errors near the ice edge and regions dominated by thin ice (such as the Sea of Okhotsk). Validation studies indicate that the Bootstrap algorithm is more sensitive to thin ice, and therefore more accurate in those regions than the NASA Team algorithm (Partington, 2000).

B. Sea ice surface variability impacts the brightness temperature signal, including snow cover, frost flowers, and variations in ice salinity. During winter conditions,

these effects are generally small, resulting in average concentration errors of a few percent (Gloersen et al., 1993), though higher errors can occur and are most often underestimated. For example, a comparison between passive microwave sea ice concentrations and concentration derived from high-resolution SAR scenes found that SAR showed less than 0.5% open water area in winter mid-pack sea ice while Bootstrap and NASA Team estimates had 1-3% open water.

Algorithms have been developed to also employ the higher frequency channels (85.5 GHz on SSM/I) to provide additional information (Markus and Cavalieri, 2000; Spreen et al., 2008). However, these algorithms typically require ancillary atmospheric data and/or radiative transfer modeling because the high frequency channels are more sensitive to atmospheric emissions. Also, the high frequency data have anomalies in the early part of the time series, limiting the length of the record, and unlike the lower frequency channels, are not available at all for the 1978-1987 SMMR record.

C. Physical temperature can cause errors in sea ice retrieval. Brightness temperature is a function of both the surface emissivity and the physical temperature. So, changes in physical temperature change the retrieved brightness temperature and hence the concentration. The algorithm tie-points implicitly account for a physical temperature, but large variations in temperature can cause errors. The Bootstrap algorithm concentrations are biased low in extremely cold conditions, typically during the mid-winter season in the high Arctic and near the Antarctic coast. Use of daily tie-points limits this effect, but estimates are still biased low. The NASA Team algorithm uses brightness temperature ratios, so the effect of physical temperature largely cancels out within the algorithm equations.

D. Surface melt is the largest surface effect on the retrieved concentration accuracy. When melt ponds form on the surface of ice floes in the summer, the microwave emission changes significantly because of the different emissive properties of water in the frozen state versus the liquid state (Eppler et al., 1992). The brightness temperature values over melting snow and ice are effectively interpreted by the algorithms as a mixture of sea ice and open water, so the ice concentration appears to decline when in fact the true concentration may not have changed (Fetterer and Untersteiner, 1998). Melt state is a surface effect that may in itself contain a climate trend (Markus et al., 2009), which could influence sea ice concentration trend estimates. The effect is further exacerbated when melt ponds form on the surface of the ice. Therefore, a substantial low bias in summer concentrations of 20-30% from both NASA Team and Bootstrap algorithms has been found in numerous studies (Agnew and Howell, 2003; Gloersen et al., 1993; Cavalieri, 1994; Comiso et al., 1997; Partington, 2000; Meier, 2005)

4.2.6 Errors Due to Atmospheric Effects

A significant advantage of passive microwave data for sea ice concentration retrieval is that atmospheric emission is typically low in the frequencies used in the algorithms. This provides all-sky capabilities and allows satellite passive microwave sensors to obtain complete, daily sea ice concentration fields no matter the weather or the season.

However, while atmospheric emission or atmosphere-induced surface emission is typically small, it can cause significant errors in some situations. The atmosphere primarily affects the algorithms over open water and thin ice.

One effect is not direct emission by the atmosphere but an induced effect. Wind blowing over the ocean roughens the surface, which increases its emission. Even a relatively light wind (for example, 5 m/s) can increase emission enough to register several percent concentration of sea ice when no ice is present (Gloersen et al., 1993; Andersen et al., 2006). The use of weather filters and a 15% concentration threshold eliminate most, but not all, wind effects.

The primary atmospheric emission sources are water vapor and liquid water in clouds. These sources also increase the emission retrieved by the sensor and serve to erroneously increase ice concentration. Sensitivity studies for SSM/I and SSMIS indicate that these effects can be up to a 10-20% concentration bias for open water, with decreasing effects as sea ice concentration increases (Maslanik, 1992; Oelke, 1997; Andersen et al., 2006). Such effects are primarily limited to open water and near-edge sea ice grid cells. The weather filters and the 15% threshold remove much of the effect over water, but some artifacts may remain.

5. Practical Considerations

5.1 Numerical Computation Considerations

No parallelization or difficulties in matrix inversions are expected. Round-off errors exist in conversions between data types (floating point to byte and the reverse), but these are expected and well within the tolerance of the current algorithm and instrument accuracy.

5.2 Programming and Procedural Considerations

The initial daily data can be generated in parallel, along with the temporal interpolation step. Generation of the day-of-melt parameter is a post processing step and is currently not able to be run in parallel.

The code is implemented in the Python computer language and utilizes the Conda platform for managing dependencies on packages like numpy and xarray. Pytest is used for testing. The code base is split into three packages: seaice_ecdr, pm_icecon, and pm_tb_data. These are available from GitHub. For a complete set of requirements

and environment considerations, see the environment.yml file in each of the packages available at the following GitHub URLs:

- seaice_ecdr: https://github.com/nsidc/seaice_ecdr
- pm_icecon: https://github.com/nsidc/pm_icecon
- pm_tb_data: https://github.com/nsidc/pm_tb_data

The complete source code package can also be downloaded as a zip file from the NOAA NCEI Sea Ice Concentration CDR web page: https://www.ncei.noaa.gov/products/climate-data-records/sea-ice-concentration.

5.3 Quality Assessment and Diagnostics

Researchers can independently reproduce, assess, and improve a CDR by comparing it with operational products of known science quality (i.e., uncertainty). Errors can be estimated via comparison to operational sea ice products, such as those produced by the U.S. National Ice Center (USNIC) or the Canadian Ice Service (CIS). It is important to keep in mind that such products have an operational focus different from the climate focus of the CDR, and the two are not necessarily internally consistent with each other. Operational ice charts meet the needs of those going into the ice and provide general situational awareness, such as the extent of fast ice or of ice of any concentration greater than zero percent. Chart production is flexible in order to meet changing user needs and source data availability. USNIC chart products, for example, usually represent sea ice more accurately than products based on single-sensor satellite data alone. For any given region or day, a user who wants the most accurate analysis of ice edge position and concentration should use products from an operational ice service such as the USNIC or CIS. Ice charts are used to make *U.S. National Ice Center Arctic and Antarctic Sea Ice Concentration and Climatologies in Gridded Format* (U.S. National Ice Center, 2020).

While operational analyses are usually the most accurate and timely representation of sea ice, they have errors and biases that change over time. If one is interested in long-term trends in sea ice or how it responds to changing climate forcing, generally, it is best not to use an operational product, but rather one that is consistently produced and retroactively quality controlled such as this SIC CDR. Section 4.2.3 describes error assessments between operational products and passive microwave sea ice concentrations.

5.4 Exception Handling

Error cases in the code are caught and informative error messages are printed on exit and saved to a log file on disk where they can be viewed later if needed. Examples of these error cases are a warning about missing data for a prior day when doing temporal interpolation or if there is no data found around the pole hole for spatial averaging. These errors are used to investigate anomalies in the data processing or data file output.

5.5 Processing Environment and Resources

Data were processed on virtual machines provisioned with all code dependencies using NSIDC cyber-infrastructure.

5.5.1 Look-Up Table Description

Within the code package, there are static ancillary grids and configuration files used to create this product. The ancillary files consist of data grids and masks necessary to perform automated quality controls. The configuration files provide information to the code on the dates to switch satellites and how to handle missing data. These files are described below. For an in-depth description of the purpose of the ancillary data, see Section 3.3.2.

5.5.1.1 V6 CDR Ancillary Files

There are two sets of ancillary files: ones used for the entire time series and ones used for the SMMR-era data only.

5.5.1.1.1 Entire Time Series Ancillary Files

There are two of these files, one for each hemisphere: (1) G02202-ancillary-psn25-v06r00.nc and (2) G02202-ancillary-pss25-v06r00.nc. These ancillary netCDF files contain the masks and grids that are used during the calculation of CDR sea ice concentration data. These are described in Table 11.

Mask/Grid	Description
adj123	Land adjacency mask that describes how far an ocean pixel is from land. The options are 1 grid cell from land, 2 grid cells from land, 3 grid cells from land, or not near land (>3 grid cells). It is used for the BT and NT2 land-spillover correction.
am2_cdr_seaice_conc_threshold	The daily sea ice concentration threshold used when calibrating the AMSR2 data using the Seki et al. (2024) method. See section 3.4.3 for details on the calculation of these values.
crs	Coordinate reference system description of the polar stereographic projection.
doy	Day of year index for the am2_cdr_seaice_conc_threshold variable.
invalid_ice_mask	An invalid ice mask that denotes areas of the grid that should not contain sea ice based on climatological analyses of seasonal sea ice locations. There are 12 masks (one for each month). This variable is used in combination with the month variable to differentiate the different monthly masks.

Mask/Grid	Description
l90c	A mask that defines the coast (land adjacent to water) as 90% sea ice concentration. This mask is needed in the calculation of the NT2 land-spillover correction.
latitude	Latitude of each grid cell in degrees north.
longitude	Longitude of each grid cell in degrees east.
month	The 12 months of the year. Used in combination with the invalid_ice_mask variable to differentiate the different monthly masks.
polehole_bitmask (Northern Hemisphere only)	This is a bitmask that maps the different pole holes for each satellite/sensor used in the creation of the CDR and applies to the northern hemisphere only. This is used for masking out the northern hemisphere pole hole – an area of the earth that is not measured by the sensor due to its earth incidence angle. Because this is a bitmask, the values are additive. For example, the SSMIS pole hole is the smallest of the pole holes so it fits inside the others. Its value is 127 which is the sum of all the bitmask values. The values for each bit are the following: 1: Nimbus 7 SMMR pole hole 2: DMSP F08 SSM/I pole hole 4: DMSP F11 SSM/I pole hole 8: DMSP F13 SSM/I pole hole 16: DMSP F17 SSMIS pole hole 32: Aqua AMSR-E pole hole (not used in this product) 64: GCOM-W1 AMSR2 pole hole
surface_type	This is a land surface type mask. It defines the following surface types: 50: ocean 75: lake 200: coast (land adjacent to ocean) 250: land
x	The x coordinate of the projection.
y	The y coordinate of the projection.

Table 11. CDR Ancillary Files Content Description

The files reside here:

```
v06r00_ancillary/
      G02202-ancillary-psn25-v06r00.nc
      G02202-ancillary-pss25-v06r00.nc
```

5.5.1.1.2 SMMR Daily Climatology Invalid Ice Masks

There are two of these files, one for each hemisphere: (1) G02202-ancillary-psn25-daily-invalid-ice-v06r00.nc and (2) G02202-ancillary-pss25-daily-invalid-ice-v06r00.nc. These are day-of-year climatology invalid ice masks derived from the GSFC Bootstrap algorithm data (Comiso, 2023). These are needed to remove weather effects in ice concentration from SMMR data because the 22 GHz channel that is used for weather filtering for the other sensors did not produce reliable data for SMMR. See section 3.4.1.4.2 for information on how these are derived.

```
v06r00_ancillary/
      G02202-ancillary-psn25-daily-invalid-ice-v06r00.nc
      G02202-ancillary-pss25-daily-invalid-ice-v06r00.nc
```

5.5.1.2 Configuration Files

There are three configuration files: (1) dates_handled_differently.yml, (2) nrt_am2_platform_start_dates.yml, and (3) default_platform_start_dates.yml. These files tell the code which satellites to use for both the final product (TCDR) and the NRT product (ICDR) as well as how to handle missing data.

The files reside here:

```
config/
      dates_handled_differently.yml
      nrt_platform_start_dates.yml
      default_platform_start_dates.yml
```

6. Assumptions and Limitations

As noted elsewhere, a primary limitation is the spatial resolution (sensor footprint) of the input data, which limits the detail that can be retrieved by the algorithm. The product is on a 25 km (nominal) resolution grid, the precision of the ice edge location is limited to ~25 km at best. Also, the resolution of the input data varies by the instrument channel. The 19 GHz channel has the largest footprint of ~70 km x ~45 km. This means that small-scale features are not explicitly resolved by the algorithm. This is generally not sufficient for operational support (for example, navigational guidance) and the product should not be used for such purposes. The primary application of the product is for long-term climate monitoring and general guidance on overall regional and global sea ice concentrations, not for operational and/or local applications.

6.1 Algorithm Performance

The algorithm is empirically derived based on the microwave emission of pure surface types. Because of the number of sensor frequency and polarization combinations that

are completely independent, only three surface types can be discriminated by the algorithm – two for sea ice and one for open water. However, the sea ice surface is highly heterogeneous. The microwave signature of ice varies based on ice thickness (up to ~50 cm), snow cover, and melt state. For a global, long-term algorithm, the algorithm is tuned to thick, cold sea ice conditions. This means that the algorithm tends to underperform in regions of thin ice and during melt conditions. Heavy snow cover can also impact the algorithm retrieval, especially if the snow grain size changes significantly and/or there are melt/refreeze events. Over open water, ocean waves and/or atmospheric emission (especially by liquid water clouds) can increase the surface emission signal and result in false ice retrieval. Weather filters (discussed previously in Section 3.4.1.4) have been included to ameliorate as much of these effects as possible, but occasionally some false ice can still occur.

6.2 Sensor Performance

The sensor performance is dependent on the satellite operation teams that monitor them. For DMSP, NOAA operates the satellites in cooperation with the U.S. Airforce. Data are downloaded from the satellites and monitored by the U.S. Navy at the Fleet Numerical Meteorology and Oceanography Center (FNMOC). For the AMSR2 L1R data, JAXA operates the satellite.

Radiometric calibration between sensor transitions is corrected by the sensor-specific tie-point adjustments used by the algorithms (see Section 3.4.2), but changes in calibration within a sensor are not addressed.

At NSIDC, the sea ice concentration fields are monitored by reviewing validation logs that give statistics about outlier data and plotting sea ice extent and looking for errant values. Sudden changes in either of these are an indication of changes in calibration or some other sensor malfunction. Generally, these spurious changes have been short-lived, but if they become chronic, the algorithm can be transitioned to use a new sensor. Thus far, radiometric noise for the passive microwave sensors has not been an issue.

7. Future Enhancements

Other enhancements in the sea ice concentration CDR will be considered for the future, pending available funding. Some of the main potential enhancements are discussed below.

7.1.1 Reprocessing Using a New Version of Brightness Temperatures

The current CDR product is based on multiple versions of brightness temperature data for SSM/I and SSMIS from Remote Sensing Systems (RSS). The intersensor adjustments between F13 and F17 were made using these versions of brightness temperatures, so any differences in RSS versions should be accounted for within the

algorithm intersensor adjustments. However, the authors aim to do a full reprocessing with a consistent, updated brightness temperature product. The NASA Global Precipitation Mission (GPM) Level 1C (L1C) dataset provides fully intercalibration brightness temperatures for all SSMI and SSMIS instruments (NASA GSFC and X-CAL Working Group, 2022). We will investigate these products for a potential full reprocessing of the sea ice product when resources allow.

7.1.2 EASE-Grid 2.0 Version of Sea Ice CDR

The NASA Making Earth Science Data Records for Use in Research Environments (MEaSUREs) enhanced EASE-Grid 2.0 (EASE2) gridded product (Brodzik et al., 2024) uses swath brightness temperatures based on the L1C processing and is currently being updated to use the latest L1C. This MEaSUREs product uses the L1C T_B swath data to create twice-daily brightness temperature composites on the EASE2 grid, including enhanced resolution fields. These brightness temperatures are now being routinely processed by the NASA DAAC at NSIDC and ongoing production, including near-real-time fields, is being supported. These would provide a suitable source of already-gridded fields. The EASE2 grid is equal area, which is easier to work with, and it includes standard geographic parameters (ellipsoid, datum, etc.) that make the data more compatible with modern software packages such as Python and GIS.

7.1.3 New Algorithm Coefficients for Calibration

While intercalibration has been done on the current input data and algorithm coefficients (tie-points) – by satellite for NASA Team and daily for Bootstrap – further adjustments may be necessary for transitions to new instruments. The approach would follow the Bootstrap methodology of daily-varying tie-points, with adaptations for the NASA Team.

7.1.4 Improved Pole-Hole Filling

The current pole-hole fill is a simple average, based on the average concentration of surrounding cells. This provides a reasonable gap-fill but does not include any spatial variability. We may investigate new methods to add realistic spatial variability to the pole hole.

7.1.5 Fill Remaining Temporal Gaps Using Statistical Modeling

While the temporal and spatial interpolation fills most gaps, there are still some periods that do not have data, most notably, Dec 1987 and Jan 1988. This is a large time gap where simple temporal interpolation is not reasonable. However, more advanced methods are possible, including statistical modeling approaches. We may investigate such methods to fill that 1987-1988 gap and other smaller remaining gaps. Because the gap is so large and the method will be unique, we may decide to provide this as an ancillary product so that users more clearly understand that that period is missing data and the data during that period is based on statistical modeling.

8. References

Agnew, T., & Howell, S. (2003). The use of operational ice charts for evaluating passive microwave ice concentration data. *Atmos. Ocean*, 41(4): 317-331.

Andersen, S., Tonboe, R., Kaleschke, L., Heygster, G., & Pedersen, L.T. (2007). Intercomparison of passive microwave sea ice concentration retrievals over the high-concentration Arctic sea ice. *J. Geophys. Res.*, 112, C08004. doi: https://doi.org/10.1029/2006JC003543.

Andersen, S., Tonboe, R., Kern, S., & Schyberg, H. (2006). Improved retrieval of sea ice total concentration from spaceborne passive microwave observations using numerical weather prediction model fields: An intercomparison of nine algorithms. *Rem. Sens. Env.*, 104: 374-392.

Belchansky, G.I. & Douglas, D.C. (2002). Seasonal comparisons of sea ice concentration estimates derived from SSM/I, OKEAN, and RADARSAT data. *Rem. Sens. Environ*., 81: 67-81.

Bliss, A.C., Anderson, M., & Drobot, S. (2022). Snow Melt Onset Over Arctic Sea Ice from SMMR and SSM/I-SSMIS Brightness Temperatures. (NSIDC-0105, Version 5). [Data Set]. Boulder, Colorado USA. NASA National Snow and Ice Data Center Distributed Active Archive Center. doi: https://doi.org/10.5067/TRGWQ0ONTQG5.

Brodzik, M.J., Long, D.G., & Hardman, M.A. (2024). Calibrated Enhanced-Resolution Passive Microwave Daily EASE-Grid 2.0 Brightness Temperature ESDR. (NSIDC-0630, Version 2). [Data Set]. Boulder, Colorado USA. NASA National Snow and Ice Data Center Distributed Active Archive Center. doi: https://doi.org/10.5067/19LHYLUXZ22M.

Cavalieri, D., Parkinson, C., DiGirolamo, N., & Ivanov, A. (2011). Intersensor calibration between F13 SSM/I and F17 SSMIS for global sea ice data records. *IEEE Geosci. Remote Sens. Lett*., 9(2), 233-236. doi: https://doi.org/10.1109/LGRS.2011.2166754.

Cavalieri, D., Parkinson, C., Gloersen, P., Comiso, J., & Zwally, H.J. (1999). Deriving Long-term Time Series of Sea Ice Cover from Satellite Passive-microwave Multisensor Data Sets. *J. of Geophys. Res.,* 104(C7):15,803-15,814.

Cavalieri, D., St. Germain, K.M., Swift, C.T. (1995). Reduction of weather effects in the calculation of sea-ice concentration with the DMSP SSM/I. *J. of Glac*., 41(139): 455-464. doi:10.3189/S0022143000034791.

Cavalieri, D. (1994). A microwave technique for mapping thin sea-ice. *J. Geophys. Res.*, 99(C6): 12561-12572.

Cavalieri, D.J., Crawford, J.P., Drinkwater, M.R., Eppler, D.T., Farmer, L.D., Jentz, R.R., & Wackerman C.C. (1991). Aircraft Active and Passive Microwave Validation of Sea Ice Concentration from the Defense Meteorological Satellite Program Special Sensor Microwave Imager. *J. Geophys. Res.*, 96(C12): 21989–22008.

Cavalieri, D.J., Gloersen, P., & Campbell, W.J. (1984). Determination of sea ice parameters with the NIMBUS-7 SMMR. *J. Geophys. Res*., 89(D4): 5355-5369.

Cho, K. and Naoki, K. (2023). A New Weather Filter for Reducing Weather Effect in Calculating Sea Ice Concentration from AMSR2 Data. *ISPRS Ann. Photogramm. Remote Sens. Spatial Inf. Sci.*, X-1/W1-2023: 793–798. doi: https://doi.org/10.5194/isprs-annals-X-1-W1-2023-793-2023.

Comiso, J.C. (2023). Bootstrap Sea Ice Concentrations from Nimbus-7 SMMR and DMSP SSM/I-SSMIS (NSIDC-0079, Version 4). [Data Set]. Boulder, Colorado USA. NASA National Snow and Ice Data Center Distributed Active Archive Center. doi: https://doi.org/10.5067/X5LG68MH013O.

Comiso, J.C., Gersten, R.A., Stock, L.V., Turner, J., Perez, G.J., & Cho, K. (2017). Positive Trend in the Antarctic Sea Ice Cover and Associated Changes in Surface Temperature. *J. Climate*, 30, 2251–2267. doi: https://doi.org/10.1175/JCLI-D-16-0408.1.

Comiso, J.C. (2009). Enhanced Sea Ice Concentrations and Ice Extents from AMSR-E Data. *J. Rem. Sens. of Japan,* 29(1):199-215.

Comiso, J.C., & Nishio, F. (2008). Trends in the Sea Ice Cover Using Enhanced and Compatible AMSR-E, SSM/I, and SMMR Data. *J. of Geophys. Res.,* 113, C02S07. doi: https://doi.org/10.1029/2007JC0043257.

Comiso, J.C., Cavalieri, D., Parkinson, C., & Gloersen, P. (1997). Passive Microwave Algorithms for Sea Ice Concentrations: A Comparison of Two Techniques. *Rem. Sens. of the Environ.,* 60(3):357-384.

Comiso, J.C. (1986). Characteristics of arctic winter sea ice from satellite multispectral microwave observations. *J. Geophys. Res*., 91(C1): 975-994.

DiGirolamo, N., Parkinson, C.L., Cavalieri, D.J., Gloersen, P. & Zwally, H.J. (2022). Sea Ice Concentrations from Nimbus-7 SMMR and DMSP SSM/I-SSMIS Passive Microwave Data (NSIDC-0051, Version 2). [Data Set]. Boulder, Colorado USA. NASA National Snow and Ice Data Center Distributed Active Archive Center. doi: https://doi.org/10.5067/MPYG15WAA4WX.

Drobot, S. & Anderson, M. (2001). Comparison of Interannual Snowmelt Onset Dates with Atmospheric Conditions. *Annals of Glaciology* 33: 79-84.

Eppler, D.T. & 14 others (1992). Passive microwave signatures of sea ice, in "Microwave Remote Sensing of Sea Ice." F.D. Carsey, ed., *American Geophysical Union Monograph* 68, Washington, DC:47-71.

Fetterer, F., Windnagel, A., Meier, W., Stewart, J.S., & Stafford, T. (2023). AMSR2 for a Better NOAA/NSIDC Sea Ice Concentration Climate Data Record. American Meteorological Society 103rd Annual Meeting, Denver, CO, USA, 8 Jan. 2023.

Gloersen, P. (2006). Nimbus-7 SMMR Polar Gridded Radiances and Sea Ice Concentrations. (NSIDC-0007, Version 1). [Data Set]. Boulder, Colorado USA. NASA National Snow and Ice Data Center Distributed Active Archive Center. doi: https://doi.org/10.5067/QOZIVYV3V9JP.

Gloersen, P., Campbell, W.J., Cavalieri, D.J., Comiso, J.C., Parkinson, C.L., & Zwally H.J. (1993). Arctic and Antarctic sea ice, 1978-1987: Satellite passive-microwave observations and analysis. *NASA Spec. Publ.* 511, 290 pp.

Gloersen, P. & Hardis, L. (1978)**.** The Scanning Multichannel Microwave Radiometer (SMMR) experiment. *The Nimbus 7 Users' Guide.* C. R. Madrid, editor. National Aeronautics and Space Administration. Goddard Space Flight Center, Maryland.

Gloersen, P. & Barath, F.T. (1977). A Scanning Multichannel Microwave Radiometer for Nimbus-G and SeaSat-A. *IEEE Journal of Oceanic Engineering* 2:172-178.

Hallikainen, M. & Winebrenner, D.P. (1992). The physical basis for sea ice remote sensing, in "Microwave Remote Sensing of Sea Ice", F.D. Carsey, ed., *American Geophysical Union Monograph* 68, Washington, DC:29-46.

Hollinger, J.P., Peirce, J.L., & Poe, G.A. (1990). "SSM/I instrument evaluation," in *IEEE Transactions on Geoscience and Remote Sensing*, vol. 28, no. 5, pp. 781-790. doi: https://doi.org/10.1109/36.58964.

Imaoka, K., Kachi, M., Kasahara, M., Ito, N., Nakagawa, K., & Oki, T. (2010). Instrument performance and calibration of AMSR-E and AMSR2. *International archives of the photogrammetry, remote sensing and spatial information science*, 38(8), 13-18.

Ishikawa, T., Noguchi, T., Yokobori, S., Ito, T., Taniguchi, M., Okada, Y., & Kasahara, M. (2017). On-orbit performance of High Temperature Noise Source (HTS) for advanced microwave scanning radiometer 2 (AMSR2) onboard the GCOM-W satellite. In *2017 IEEE International Geoscience and Remote Sensing Symposium (IGARSS)* (pp. 522-525). IEEE.

Kawanishi, T. & 9 others. (2003). The Advanced Microwave Scanning Radiometer for the Earth Observing System (AMSR-E), NASDA's contribution to the EOS for global energy and water cycle studies. *IEEE Transactions on Geoscience and Remote Sensing*, 41(2), 184-194. doi: https://doi.org/10.1109/TGRS.2002.808331.

Kern, S., Lavergne, T., Notz, D., Pedersen, L.T., & Tonboe, R. (2020). Satellite passive microwave sea-ice concentration data set inter-comparison for Arctic summer conditions. *The Cryosphere*, 14(7), 2469-2493.

Kern, S., Lavergne, T., Notz, D., Pedersen, L.T., Tonboe, R.T., Saldo, R., & Sørensen, A.M. (2019). Satellite passive microwave sea-ice concentration data set intercomparison: closed ice and ship-based observations. *The Cryosphere*, 13(12), 3261-3307.

Kunkee, D.B., Poe, G.A., Boucher, D.J., Swadley, S.D., Hong, Y., Wessel, J.E., & Uliana, E.A. (2008). Design and evaluation of the first Special Sensor Microwave Imager/Sounder. *IEEE Trans. Geosci. Remote Sens.*, 46(4), 863-883.

Kwok, R. (2002). Sea ice concentration estimates from satellite passive microwave radiometry and openings from SAR ice motion. *Geophys. Res. Lett.*, 29(9), 1311. doi: https://doi.org/10.1029/2002GL014787.

Levitus, S. & Boyer, T.P (1994). World Ocean Atlas 1994, Volume 4: Temperature, NOAA National Oceanographic Data Center, Ocean Climate Laboratory, U.S. Department of Commerce, Washington D.C.

Liu, Yinghui, & Key, Jeffrey R. (2019). NOAA/NESDIS Center for Satellite Applications and Research, Algorithm Theoretical Basis Document: Ice Surface Temperature, Ice Concentration, and Ice Cover, Version 1.2. Accessed 10 December 2024 from https://www.star.nesdis.noaa.gov/goesr/documents/ATBDs/Baseline/ATBD_GOES-R_IceConcentration_v1.2_Feb2019.pdf.

Markus, T. & Cavalieri, D.J. (2009). The AMSR-E NT2 Sea Ice Concentration Algorithm: its Basis and Implementation. *J. of the Rem. Sens. Soc. of Japan*, 29(1): 216-225.

Markus, T., Stroeve, J.C., & Miller, J. (2009). Recent changes in Arctic sea ice melt onset, freezeup, and melt season length. *J. Geophys. Res.*, 114, C12024. doi: https://doi.org/10.1029/2009JC005436.

Markus, T., & Cavalieri, D.J. (2000). An enhancement of the NASA Team sea ice algorithm. *IEEE Trans. Geosci. Remote Sens.*, 38(3): 1387-1398.

Maslanik, J. (1992). Effects of weather on the retrieval of sea ice concentration and ice type from passive microwave data. *Int. J. Remote Sens.*, 13(1): 37-54.

Meier, W.N., Fetterer, F., Windnagel, A.K., Stewart, J.S., & Stafford, T. (2026a). NOAA/NSIDC Climate Data Record of Passive Microwave Sea Ice Concentration. (G02202, Version 6). [Data Set]. Boulder, Colorado USA. National Snow and Ice Data Center. doi: https://doi.org/10.7265/b18j-z797.

Meier, W.N., Fetterer, F., Windnagel, A.K. Stewart, J.S., & Stafford T. (2026b). Near-Real-Time NOAA/NSIDC Climate Data Record of Passive Microwave Sea Ice

Concentration. (G10016, Version 4). [Data Set]. Boulder, Colorado USA. National Snow and Ice Data Center. doi: https://doi.org/10.7265/tm2n-1m33.

Meier, W.N., Stewart, J.S., Wilcox, H., Scott, D.J. & Hardman, M.A. (2021). DMSP SSM/I-SSMIS Daily Polar Gridded Brightness Temperatures. (NSIDC-0001, Version 6). [Data Set]. Boulder, Colorado USA. NASA National Snow and Ice Data Center Distributed Active Archive Center. doi: https://doi.org/10.5067/MXJL42WSXTS1.

Meier, W.N., Stewart, J.S., Liu, Y., Key, J., & Miller, J.A. (2017). An operational implementation of sea ice concentration estimates from the AMSR2 sensor. *IEEE J. Sel. Topics Appl. Earth Obs. & Rem. Sens.* 10(9) doi: https://doi.org/10.1109/JSTARS.2017.2693120.

Meier, W.N., Stroeve, J., Fetterer, F., Savoie, M., & Wilcox, H. (2015). Polar Stereographic Valid Ice Masks Derived from National Ice Center Monthly Sea Ice Climatologies. (NSIDC-0622, Version 1). [Data Set]. Boulder, Colorado USA. NASA National Snow and Ice Data Center Distributed Active Archive Center. doi: https://doi.org/10.5067/M4PUJAQRI2DS.

Meier, W.N., Peng, G., Scott, D.J., & Savoie, M.H. (2014). Verification of a new NOAA/NSIDC passive microwave sea-ice concentration climate record. *Polar Res.*, 33. doi: https://doi.org/10.3402/polar.v33.21004.

Meier, W.N. & Khalsa, S.J.S. (2011). Intersensor calibration between F-13 SSM/I and F-17 SSMIS Near-Real-Time Sea Ice Estimates. *Geosci. and Remote Sens.,* 49(9): 3343-3349.

Meier, W.N. (2005). Comparison of passive microwave ice concentration algorithm retrievals with AVHRR imagery in Arctic peripheral seas. *IEEE Trans. Geosci. Remote Sens.*, 43(6): 1324-1337.

Meier, W.N., Maksym, T., & Van Woert, M. (2003). Evaluation of Arctic operational passive microwave products: A case study in the Barents Sea during October 2001. “Ice in Environment: Proceedings of the 16th International Association of Hydraulic Engineering and Research”, Dunedin, NZ, 2-6 Dec. 2002, vol. 3:213-222.

Nakagawa, K. (2010). Global Change Observation Mission (GCOM). International Archives of the Photogrammetry, Remote Sensing and Spatial Information Science, Volume XXXVIII.

NAS (2004). Climate data records from environmental satellites: Interim report, National Academies of Science (NAS), National Academies Press, Washington, D.C., 150 pp.

NASA Goddard & X-CAL Working Group. (2022). Precipitation Processing System (PPS) Precipitation Processing System (PPS) Algorithm Theoretical Basis Document (ATBD) NASA Global Precipitation Measurement (GPM) Level 1C Algorithms, Version 1.9. Goddard Space Flight Center. Greenbelt, Maryland.

https://pps.gsfc.nasa.gov/Documents/L1C_ATBD_v1.9_GPMV07.pdf. Accessed November 2024.

Oelke, C. (1997). Atmospheric signatures in sea-ice concentration estimates from passive microwaves: Modelled and observed. *Int. J. Remote Sens*., 18(5): 1113-1136.

Ozsoy-Cicek, B., Ackley, S.F., Worby, A., Xie, H., & Lieser, J. (2011). Antarctic sea-ice extents and concentrations: Comparison of satellite and ship measurements from International Polar Year cruises. *Ann. Glaciol*., 52(57): 318-326.

Ozsoy-Cicek, B., Xie, H., Ackley, S.F., & Ye, K. (2009). Antarctic summer ice concentrations and extent: Comparison of ODEN 2006 ship observations and NIC sea ice charts. *The Cryosphere*, 3: 1-9.

Partington, K., Flynn, T., Lamb, D., Bertoia, C., & Dedrick, K. (2003). Late twentieth century Northern Hemisphere sea-ice record from U.S. National Ice Center ice charts. *J. Geophys. Res*., 108(C11): 3343. doi: https://doi.org/10.1029/2002JC001623.

Partington, K.C. (2000). A data fusion algorithm for mapping sea-ice concentrations from Special Sensor Microwave/Imager data. *IEEE Trans. Geosci. Remote Sens*., 38(4): 1947-1958.

Peng, G., Meier, W.N., Scott, D.J., & Savoie, M.H. (2013). A long-term and reproducible passive microwave sea ice concentration data record for climate studies and monitoring. *Earth Sys. Sci. Data*, 5, 311-318. doi: https://doi.org/10.5194/essd-5-311-2013.

Seki, M., Hori, M., Naoki, K., Kachi, M., Imaoka, K. (2024). Intersensor Calibration of Spaceborne Passive Microwave Radiometers and Algorithm Tuning for Long-Term Sea Ice Trend Analysis Based on AMSR-E Observations. Remote Sens. **(**16) 3549. https://doi.org/10.3390/rs16193549.

Spreen, G., Kaleschke, L., & Heygster, G. (2008). Sea ice remote sensing using AMSR-E 89-GHz channels. *J. Geophys. Res*., 113, C02S03. doi: https://doi.org/10.1029/2005JC003384.

Steffen, K., Key, J., Cavalieri, D.J., Comiso, J., Gloersen, P., St. Germain, K., *and* Rubinstein, I. (1992). The estimation of geophysical parameters using passive microwave algorithms, in “Microwave Remote Sensing of Sea Ice.” F.D. Carsey, ed., American Geophysical Union Monograph 68, Washington, DC:201-231.

Stewart, J. S., Meier, W. N., Wilcox, H., Scott, D. J. & Marowitz, R. (2025). AMSR2 Daily Polar Gridded Brightness Temperatures. (NSIDC-0802, Version 2). [Data Set]. Boulder, Colorado USA. National Snow and Ice Data Center. https://doi.org/10.5067/DEYP05J7GMSH.

U.S. National Ice Center. (2006). U.S. National Ice Center Arctic Sea Ice Charts and Climatologies in Gridded Format, 1972 - 2007. (G02172, Version 1). Fetterer, F. & Fowler, C. (Comps.) Boulder, Colorado USA. National Snow and Ice Data Center. https://doi.org/10.7265/N5X34VDB.

Wentz, F.J. (1997). A well-calibrated ocean algorithm for SSM/I. *J. Geophys. Res.*, 102(C4): 8703-8718.

Willmes, S., Haas, C., Nicolaus, M., & Bareiss, J. (2009). Satellite microwave observations of the interannual variability of snowmelt on sea ice in the Southern Ocean. *J. Geophys. Res.*, 114, C03006. doi: https://doi.org/10.1029/2008JC004919.

Zwally, H.J., Comiso, J.C., Parkinson, C.L., Campbell, W.J., Carsey, F.D., & Gloersen, P. (1983). Antarctic sea ice 1973-1976 from satellite passive microwave observations. *NASA Spec. Publ.*, 459, 206 pp.

Appendix A - ACRONYMS AND ABBREVIATIONS

Acronym	Meaning
AMSR-E	Advanced Microwave Scanning Radiometer for EOS
AMSR2	Advanced Microwave Scanning Radiometer 2
BT	Bootstrap
CATBD	Climate Algorithm Theoretical Basis Document
CDR	Climate Data Record
CLASS	Comprehensive Large Array-data Stewardship System
DAAC	Distributed Active Archive Center
DMSP	Defense Meteorological Satellite Program
DOY	Day of Year
ECDR	Enhanced Climate Data Record
ICDR	Interim Climate Data Record
IFOV	Instantaneous Field of View
FY	First-year
GCOM	Global Change Observation Mission
GSFC	Goddard Space Flight Center
H	Horizontal
ICDR	Interim Climate Data Record
MEaSUREs	NASA Making Earth Science Data Records for Use in Research Environments
MY	Multiyear
NAS	National Academies of Science
NASA	National Aeronautics and Space Administration
NCEI	National Center for Environmental Information
NOAA	National Oceanic and Atmospheres Administration
NSIDC	National Snow and Ice Data Center
NRT	Near Real Time
NT	NASA Team
OW	Open Water
QC	Quality Control
RSS	Remote Sensing Systems, Inc.
SMMR	Scanning Multichannel Microwave Radiometer
SSM/I	Special Sensor Microwave Imager
SSMIS	Special Sensor Microwave Imager/Sounder
SST	Sea Surface Temperature
TCDR	Thematic Climate Data Record
V	Vertical